障害説も提唱されている．

II. 細胞膜の脆弱性とCa^{2+}イオン透過性亢進の分子機構

従来からDMDの病態として細胞膜仮説，すなわち細胞膜の脆弱性と細胞内へのCa^{2+}イオンの流入とプロテアーゼの活性化により筋細胞壊死が生じると考えられていた．ミシガン大学Metzger教授のグループはジストロフィン欠損心筋細胞を単離しマイクロカーボンを用いて筋節長だけ伸展させ，発生する張力と細胞内Ca^{2+}濃度を測定した[1]．ジストロフィン欠損心筋細胞では伸長により細胞内へCa^{2+}が流入して，過収縮が起こり心筋細胞の死滅が観察された．このようにジストロフィン欠損筋で伸長によりCa^{2+}イオンが細胞内へ流入するチャネルについては長い間わかっていなかった．最近Iwataら[2]は，ストレッチ感受性イオンチャネルであるTRPV2がCa^{2+}イオン流入のpathwayであることを見いだした．正常な骨格筋ではTRPV2は細胞質内の膜系に局在しているが，ジストロフィン欠損筋では筋鞘膜に濃縮して局在するようになる．そこで彼らは筋鞘膜に局在したTRPV2が活性化して細胞内Ca^{2+}濃度が上昇する結果，筋細胞が壊死に陥るとの作業仮説を考えた．この仮説を検証するため，ドミナントネガティブ変異を導入してTRPV2を不活化したトランスジェニックマウスを作出し，*mdx*マウスと交配して筋肉の変化を解析した．TRPV2を特異的に阻害した*mdx*マウスでは，筋細胞の壊死や線維化が有意に抑制され，筋ジストロフィー変化が改善することが示された．したがって，TRPV2の特異的な阻害薬が開発されればジストロフィノパチーの有効な治療薬として期待される．

III. 膜修復機構の異常による細胞膜の脆弱性

骨格筋は収縮と弛緩を繰り返すことから，筋鞘膜は力学的なストレスに曝されており，細胞膜が損傷を受けやすい．そこで，生体には損傷した細胞膜を修復する生理的なメカニズムが存在することが推定される．アイオワ大学のCampbellらは，三好型遠位型筋ジストロフィーやLGMD2Bの原因蛋白であるジスフェルリンが膜修復に関与することを明らかにした[3]．単一筋線維にレーザー照射により筋鞘膜損傷を与えると損傷部位にジスフェルリンが集積して，速やかに膜を修復する．一方で，ジスフェルリン欠損マウスでは膜が修復されないため，細胞外液が容易に細胞内に流入することが示された．ジスフェルリン欠損筋では損傷した筋鞘膜の直下に膜小胞が集積した像が観察されるが，修復機転において表面膜に融合できなかった小胞が集積したものと解釈できる．ジスフェルリンによる膜修復過程はCa^{2+}依存性であることが解明されている．

最近，京都大学の竹島教授のグループはジスフェルリンとは異なり，Ca^{2+}非依存性に膜修復に関与するミツグミン（MG53）という新たな分子を発見した[4]．ミツグミンのノックアウトマウスでは，筋ジストロフィー変化が観察されることから，筋ジストロフィーの発症機序への関与も推測される．また，筋ジストロフィーの新たな原因蛋白候補というだけではなく，治療薬開発の新たなシーズとしても注目されている．

IV. nNOS活性低下による血管拡張障害

熊本大学のMiikeら[5]は，電顕での観察からDMDでは早い段階から筋内血管内皮細胞が腫大して毛細血管内腔が狭小化することを指摘していた．Bredtらはジストロフィン欠損筋ではnNOSの局在が筋鞘膜から細胞質へと変化するとともに活性が低下することを見いだした[6]．しかし，nNOSノックアウトマウスでは筋障害がみられないことから，筋ジストロフィーの発症機序にnNOS活性低下がどのように関与するかは長らく不明であった．Yasuharaらは高頻度電気刺激により筋収縮運動を反復させた時，正常でみられる筋血流量の増大が*mdx*マウス（ジストロフィン欠損筋）では欠如することを見いだした[7]．さらに*mdx*マウスでは筋収縮後のNO産生が減弱していることが明らかにされた．すなわち，ジストロフィン欠損筋ではnNOS活性の減弱により筋収縮に伴う血管拡張反応を担うNO産生が低下していると推測される．そこで，NOの下流で働くcGMPを上昇させるphosphodiesterase 5（PDE5）阻害薬を*mdx*マウスに投与したところ，筋ジストロフィー変化の有意な改善が観察された．Campbellのグループも PDE5阻害薬投与により，*mdx*マウスに

おいて運動負荷後の筋血流量が顕著に増大することを示している[8].

正常な骨格筋でnNOS活性が低下しても，それだけでは筋ジストロフィーは発症しないが，ジストロフィン欠損というfirst hitの上にnNOS活性低下による筋血管拡張障害というsecond hitが加わることにより筋ジストロフィーが増悪するという，いわゆる“筋ジストロフィー発症のtwo-hit mechanism”が提唱されている.

V. RNA病としての筋ジストロフィー

スプライシングやエディティングなどのRNAプロセッシングの異常に起因する疾患はRNA病と呼ばれる．筋強直性ジストロフィーはいろいろな遺伝子のスプライシング異常によって多彩な症状を呈するRNA病であることが解明されてきた．この疾患（1型）では第19染色体のDMキナーゼ（DMPK）遺伝子の3′非翻訳領域にあるCTGリピートの異常伸長がみられるが[9]，DMPK蛋白自体には異常がない．つまり原因蛋白レベルの異常で病気が発症するわけではない．異常伸長したCTGリピートはDMPK遺伝子のRNAへの転写段階でCUGリピートとなるが，異常伸長したCUGにはMBNL1-3やCELF1-6などのRNA結合蛋白が結合する．これらのRNA結合蛋白は様々な遺伝子のmRNAへの転写過程で，スプライシングを制御している．したがって，異常伸長したCUGリピートにスプライシングを調節するRNA結合蛋白質が結合してトラップされると，正常なスプライシングの制御に支障をきたすと考えられる．この病気の特徴であるミオトニアは塩素チャネルの機能異常で生じるが，患者の筋肉では塩素チャネルCLCN1遺伝子の異常スプライシングにより幼若型CLCN1が発現している[10]．また，インスリン受容体においても，スプライシング異常により幼若型受容体が優位になっていて，おそらくインスリン耐性の原因と考えられている[11].

VI. RNAレベルの分子病態から新たな治療戦略へ

従来のような蛋白レベルの分子病態の理解だけではなくRNAレベルにおける分子病態の理解が，新たな治療法開発へのアプローチに重要になると思われる．DMDの場合DNAレベルでout-of flame欠失を修正することは困難であるが，欠失に隣接するexonをRNAへの転写段階でスプライシングによりスキップさせることでin-flame欠失に変換して軽症化を試みる，いわゆるexon skippingという治療法が注目されている．今後はDMD以外の筋ジストロフィーに対しても，このようなRNAレベルを標的とした治療戦略の応用が考えられる．したがって，重症度など臨床表現型との相関を含め，RNAレベルでの分子病態の詳細な解析が重要になると思われる.

文　献

1）Yasuda S, Townsend D, Michele DE et al : Dystrophic heart failure blocked by membrane sealant poloxamer. Nature 436 : 1025-1029, 2005

2）Iwata Y, Katanosaka Y, Arai Y et al : Dominant-negative inhibition of Ca^{2+} influx via TRPV2 ameliorates muscular dystrophy in animal models. Hum Mol Genet 18 : 824-834, 2009

3）Bansal D, Miyake K, Vogel SS et al : Defective membrane repair in dysferlin-deficient muscular dystrophy. Nature 423 : 168-172, 2003

4）Cai C, Masumiya H, Weisleder N et al : MG53 nucleates assembly of cell membrane repair machinery. Nat Cell Biol 11 : 56-64, 2009

5）Miike T, Sugino S, Ohtani Y et al : Vascular endothelial cell injury and platelet embolism in Duchenne muscular dystrophy at the preclinical stage. J Neurol Sci 82 : 67-80, 1987

6）Brenman JE, Chao DS, Xia H et al : Nitric oxide synthase complexed with dystrophin and absent from skeletal muscle sarcolemma in Duchenne muscular dystrophy. Cell 82 : 743-752, 1995

7）Asai A, Sahani N, Kaneki M et al : Primary role of functional ischemia, quantitative evidence for the two-hit mechanism, and phosphodiesterase-5 inhibitor therapy in mouse muscular dystrophy. Plos One 8 : 1-16, 2007

8）Kobayashi YM, Rader EP, Crawford RW et al : Sarcolemma-localized nNOS is required to maintain activity after mild exercise. Nature 456 : 511-515, 2008

9）Brook JD, Mila E, McCurrach HG et al : Molecular basis of myotonic dystrophy : expansion of a trinucleotide (CTG) repeat at the 3' end of a transcript encoding a protein kinase family member. Cell 68 : 799-808, 1992

10) Nezu Y, Kino Y, Sasagawa N et al : Expression of MBNL and CELF mRNA transcripts in muscles with myotonic dystrophy. Neuromuscul Disord 17 : 306-312, 2007

11) Savkur RS, Philips AV, Cooper TA : Aberrant regulation of insulin receptor alternative splicing is associated with insulin resistance in myotonic dystrophy. Nat Genet 29 : 40-47, 2001

Molecular Pathogenesis of Muscular Dystrophies

Yoshihide SUNADA

Department of Neurology, Kawasaki Medical School

Muscular dystrophy is one of the most devastating diseases for which there is no effective therapy at present. In an attempt to develop effective therapeutics, a considerable number of causative genes for the numerous types of muscular dystrophy have been identified in the last twenty years. However, uncovering causative genes alone is not enough. It is crucial to comprehend molecular pathogenesis of muscular dystrophy, focusing on the causative proteins. It is further necessary to investigate the RNA processing defects.

Muscular dystrophies can be divided into five groups depending on the subcellular localization of the causative proteins as follows : (1) the extracellular matrix proteins such as laminin $\alpha 2$ or collagen VI, (2) the sarcolemmal proteins including dystrophin, sarcoglycans, and dysferlin, (3) the sarcommeric proteins like myotilin, titin, and FHL-1, (4) the nuclear membrane proteins like emerin and lamin A/C, and (5) other miscellaneous proteins such as calpain 3 and TRIM32.

Given the number of proteins attributed to muscular dystrophy, it can be said to be a heterogeneous and variable pathogenesis. However, recent research has revealed important molecular mechanisms leading to muscle degeneration. We discuss three major issues. First, in the pathogenesis of dystrophinopathy, increased sarcolemmal fragility and increased Ca^{2+} influx have been observed. It is also revealed that TRPV2, a stretch-sensitive ion channel, plays a significant role in increasing Ca^{2+} influx. Second, dysferlin has been proved to be involved in the membrane repair system. In addition to the molecule dysferlin which works in a Ca^{2+}dependent manner, MG53 has been identified to play a significant role in membrane repair without Ca^{2+}. MG53 is also expected to be a novel therapeutic target molecule. Third, as a major underlying factor causing muscle damage in dystrophin-deficient skeletal muscle, decreased nNOS activity has been pointed. Dystrophin-deficient skeletal muscle is damaged as a consequence of disturbed vasodilation after muscle contraction. This is proved with *mdx* mice, where administration of a phosphodiesterase 5 inhibitor, a potent vasodilator, ameliorates muscle damage.

Although these findings at the protein level have great implications for the therapy of muscular dystrophy, clarifying the molecular mechanisms at the RNA level will be the key in developing novel therapeutic strategies. One of the new therapies for DMD could be the exon-skipping therapy where anti-sense agents are used to modify RNA splicing.

nature
cell biology

Mesenchymal progenitors distinct from satellite cells contribute to ectopic fat cell formation in skeletal muscle

Akiyoshi Uezumi[1,5], So-ichiro Fukada[2], Naoki Yamamoto[3], Shin'ichi Takeda[4] and Kunihiro Tsuchida[1]

Ectopic fat deposition in skeletal muscle is closely associated with several disorders, however, the origin of these adipocytes is not clear, nor is the mechanism of their formation. Satellite cells function as adult muscle stem cells but are proposed to possess multipotency. Here, we identify PDGFRα$^+$ mesenchymal progenitors as being distinct from satellite cells and located in the muscle interstitium. We show that, of the muscle-derived cell populations, only PDGFRα$^+$ cells show efficient adipogenic differentiation both *in vitro* and *in vivo*. Reciprocal transplantation between regenerating and degenerating muscles, and co-culture experiments revealed that adipogenesis of PDGFRα$^+$ cells is strongly inhibited by the presence of satellite cell-derived myofibres. These results suggest that PDGFRα$^+$ mesenchymal progenitors are the major contributor to ectopic fat cell formation in skeletal muscle, and emphasize that interaction between muscle cells and PDGFRα$^+$ mesenchymal progenitors, not the fate decision of satellite cells, has a considerable impact on muscle homeostasis.

Adult skeletal muscle possesses a remarkable regenerative ability. This depends on satellite cells that reside adjacent to and beneath the basal lamina of myofibres and function as adult muscle stem cells[1]. Despite that, in several pathological conditions where muscle integrity has been debilitated, skeletal muscle is occupied by adipocytes. The most striking accumulation of adipocytes is seen in advanced cases of Duchenne muscular dystrophy (DMD), where a muscle may be almost entirely replaced by adipocytes[2]. However, fat accumulation can be seen not only in myopathies but also in severe neurogenic atrophy, type II diabetes, obesity or ageing-related sarcopenia[3–6]. Nevertheless, the precise origin of ectopic adipocytes is not clear, and nor is the stimulus that incites their formation.

Adipose cells are thought to be derived from mesenchymal stem cells (MSCs). During adipose tissue development, MSCs commit into adipocyte lineage and eventually give rise to preadipocytes, which cannot be distinguished from MSCs by their morphology or gene expression, but have lost potential for differentiation to other cell lineages[7]. Preadipocytes then undergo terminal differentiation that involves a highly regulated and coordinated cascade of transcription factors[8]. C/EBPα and PPARγ are the best-characterized transcriptional factors for adipogenesis[9,10]. These two factors function cooperatively to transactivate adipocyte genes and continue to be expressed in mature adipocytes. Lineage commitment and differentiation of adipose progenitors or stem cells should occur in ectopic fat formation in skeletal muscle as well as in adipose tissue development. Several types of cell isolated from skeletal muscle have been reported to possess adipogenic differentiation potential including satellite cells[11,12], side population cells[13] and MSCs[14,15]. However, it is not clear whether these cells have the ability to induce *in vivo* fat formation in skeletal muscle. It is not known whether satellite cell plasticity or multipotency is operative *in vivo*, and little is known about the *in vivo* features of muscle side population cells or MSCs, such as their anatomical localization and pathophysiological roles.

Here, we conducted a comprehensive analysis of cells that reside in skeletal muscle to clarify the origin of the cell population that is involved in adipogenesis in this muscle type.

RESULTS

In vitro adipogenic potential is detected only in the PDGFRα$^+$ mesenchymal progenitor population of muscle-derived cells

We first fractionated whole mononucleated cells, which had been enzymatically isolated from skeletal muscle, based on the expression of established cell surface markers: CD31 as an endothelial marker, CD45 as a pan-haematopoietic marker and SM/C-2.6 as a marker of satellite cells (Fig. 1a)[16]. After sorting by fluorescence activated cell sorting (FACS), each cell population was cultured under adipogenic conditions to compare their adipogenic potentials (Fig. 1b). Oil red O staining revealed that only CD31$^-$CD45$^-$SM/C-2.6$^-$ cells efficiently differentiated into adipocytes (Fig. 1c). Freshly isolated CD31$^-$CD45$^-$SM/C-2.6$^-$ cells did not express endothelial, haematopoietic and myogenic genes; however, they did express *PDGFRα* and *PDGFRβ*, which have been shown to be present in mesenchymal cells (Fig. 1d)[17,18]. In particular, strong expression of *PDGFRα* was detected. When whole muscle-derived cells were fractionated on the basis of CD31,

[1]Division for Therapies against Intractable Diseases, Institute for Comprehensive Medical Science, Fujita Health University, 1-98 Dengakugakubo, Kutsukake, Toyoake, Aichi 470-1192, Japan. [2]Department of Immunology, Graduate School of Pharmaceutical Sciences, Osaka University, 1-6 Yamada-oka, Suita, Osaka 565-0871, Japan. [3]Laboratory of Molecular Biology & Histochemistry, Fujita Health University Joint Research Laboratory, Aichi 470-1192, Japan. [4]Department of Molecular Therapy, National Institute of Neuroscience, National Center of Neurology and Psychiatry (NCNP), 4-1-1 Ogawa-higashi, Kodaira, Tokyo 187-8502, Japan. [5]Correspondence should be addressed to A.U. (e-mail: uezumi@fujita-hu.ac.jp).

Received 20 May 2009; accepted 23 November 2009; published online 17 January 2010; DOI: 10.1038/ncb2014

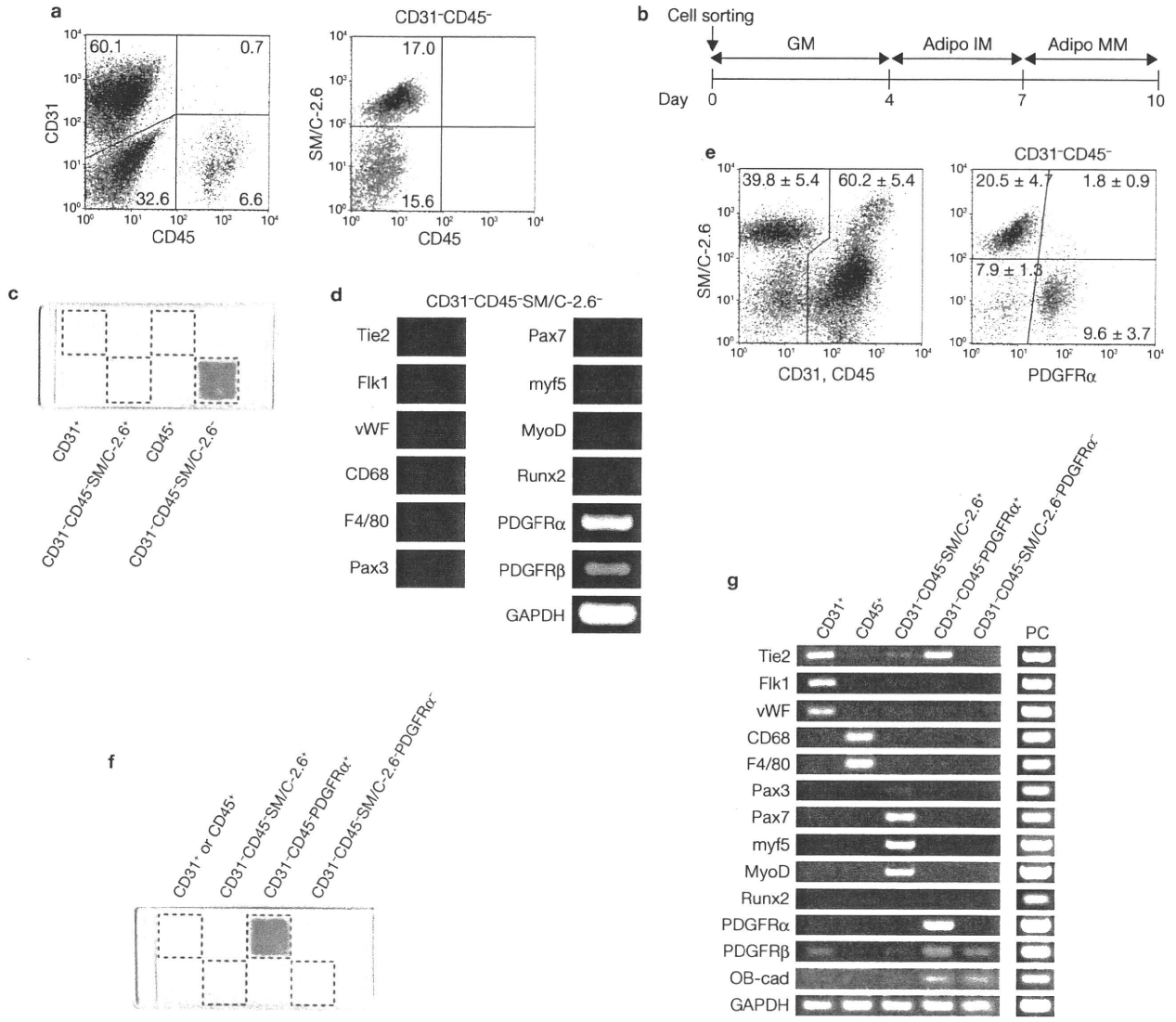

Figure 1 *In vitro* adipogenic potential was found only in the PDGFRα⁺ population of muscle-derived cells. (**a**) Whole muscle-derived cells were analysed for CD31, CD45 and SM/C-2.6 expression by flow cytometry. The percentages of each cell population are shown in the panels and expressed as the mean of three independent experiments. (**b**) Protocol for *in vitro* adipogenic differentiation. Freshly sorted cells were cultured in growth medium (GM) for 4 days before treatment with adipogenic induction medium (Adipo IM) for 3 days and treatment with adipogenic maintenance medium (Adipo MM) for 3 days. (**c**) Whole muscle-derived cells were divided into the four fractions indicated. Each fraction was cultured and induced to differentiate into adipocytes. A macroscopic view of an oil red O-stained eight-well chamber slide is shown. (**d**) RT-PCR analysis of lineage markers in freshly isolated CD31⁻CD45⁻SM/C-2.6⁻ cells. (**e**) Whole muscle-derived cells were analysed for CD31, CD45, SM/C-2.6 and PDGFRα expression. The percentages of each cell population are expressed as the mean ± s.d. of ten independent experiments. (**f**) The four fractions indicated were purified from gross muscle-derived mononucleated cells and cultured under adipogenic conditions. A macroscopic view of the oil red O stained eight-well chamber slide is shown. (**g**) Expression of lineage markers in the five fractions indicated. RNA was extracted from freshly isolated cells immediately after cell sorting and RT-PCR was performed. RNA extracted from whole embryos at embryonic day (E) 13.5 was used as a positive control (PC).

CD45, SM/C-2.6 and PDGFRα expression and induced to differentiate into adipocytes, adipogenic activity was detected only in PDGFRα⁺ cells (Fig. 1e, f). Reverse transcription-PCR (RT-PCR) analysis of freshly isolated cells showed that *PDGFRα* was specifically detected in PDGFRα⁺ cells, indicating specific expression of this molecule at both the mRNA and protein levels (Fig. 1g). In addition to the expression of mesenchymal genes, there was observable expression of the *Tie2* gene in PDGFRα⁺ cells (Fig. 1g). Tie2 has been reported to identify mesenchymal progenitors in addition to endothelial cells and a subset of haematopoietic cells[19]. Phenotypic analysis of freshly isolated PDGFRα⁺ cells revealed that they are similar to MSCs with respect to their surface phenotypes (Supplementary Information, Fig. S1a). Absence of Pax7 and adipogenic transcription factors indicated that satellite cells and committed adipogenic cells were not included in the PDGFRα⁺ fraction (Supplementary Information, Fig. S1b, c).

We next investigated *in vitro* adipogenesis of muscle-derived cell populations. Although a mixed population of CD31⁺ and CD45⁺ cells or a population of CD31⁻CD45⁻SM/C-2.6⁻PDGFRα⁻ cells proliferated poorly, two other populations, CD31⁻CD45⁻PDGFRα⁺ and CD31⁻CD45⁻SM/C-2.6⁺, proliferated actively (Fig. 2a). CD31⁻CD45⁻SM/C-2.6⁺ cells were negative for PDGFRα, C/EBPα and PPARγ (Fig. 2b), but almost all of these cells expressed Pax7 and MyoD, and a few were positive for myogenin on day 4 (Supplementary Information, Fig. S2a, d). Even upon adipogenic

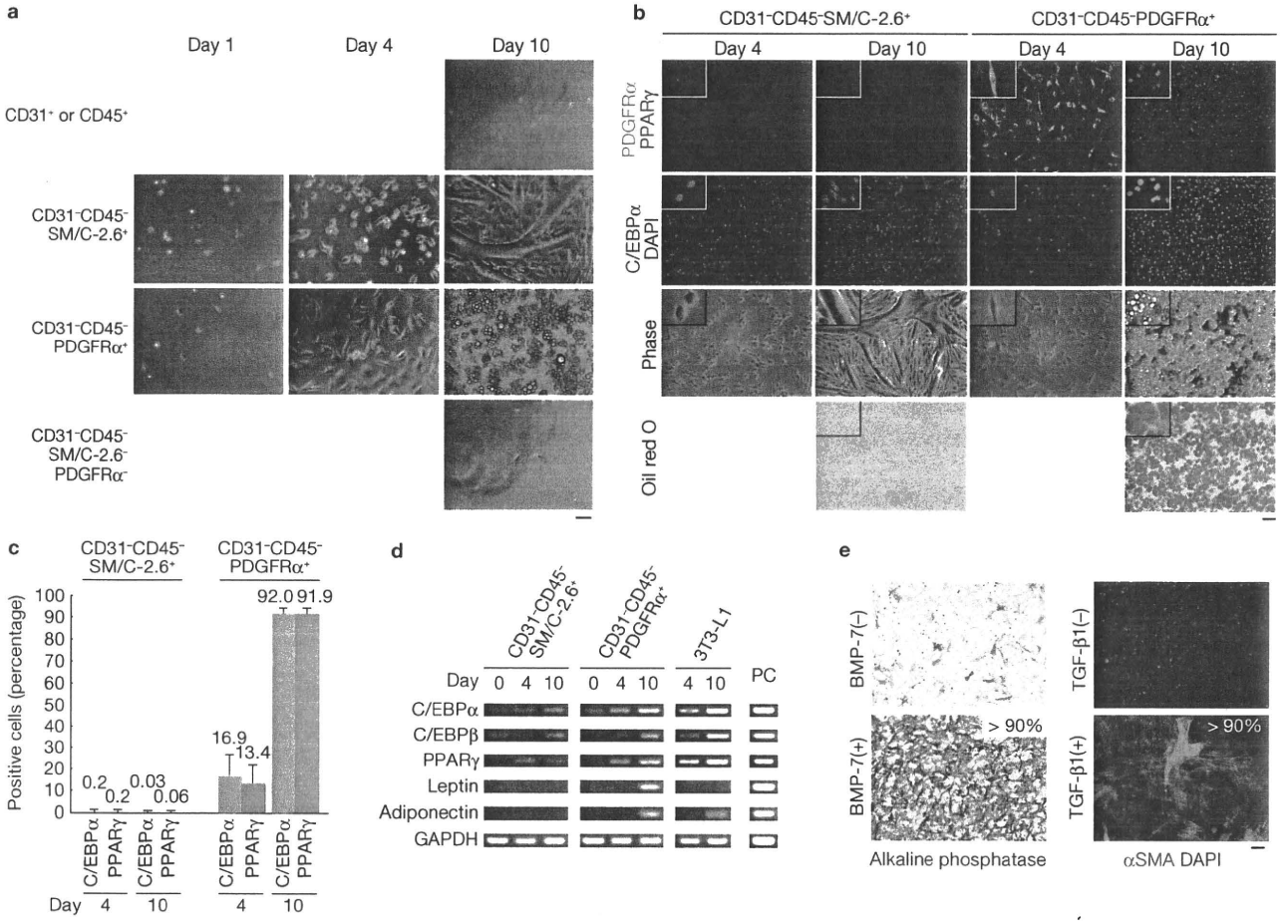

Figure 2 *In vitro* adipogenesis of muscle-derived cells. (**a**) Phase contrast images of a mixed population of CD31$^+$ and CD45$^+$ cells, CD31$^-$CD45$^-$ SM/C-2.6$^+$ cells, CD31$^-$CD45$^-$PDGFRα$^+$ cells and CD31$^-$CD45$^-$SM/C-2.6$^-$ PDGFRα$^-$ cells under adipogenic culture conditions. (**b**) Cultured CD31$^-$CD45$^-$SM/C-2.6$^+$ cells and CD31$^-$CD45$^-$PDGFRα$^+$ cells were fixed at the time points indicated and stained with antibodies against PDGFRα, C/EBPα and PPARγ, or with oil red O. Insets show high magnification images. (**c**) Adipogenic differentiation was evaluated by quantifying the percentages of C/EBPα- and PPARγ-positive cells. Error bars indicate mean ± s.d., $n = 15$ fields pulled out from three independent experiments. (**d**) Expression of adipogenic genes in CD31$^-$CD45$^-$SM/C-2.6$^+$ cells, CD31$^-$CD45$^-$PDGFRα$^+$ cells and 3T3-L1 cells during adipogenic culture. PC, positive control. (**e**) Multi-lineage differentiation of CD31$^-$CD45$^-$PDGFRα$^+$ cells. These cells were treated with BMP-7 or TGF-β1, and then alkaline phosphatase activity and αSMA expression were examined. The values in the bottom panels represent the percentages of positive cells. Scale bars, 50 μm (**a**, **b**, **e**).

induction, they did not differentiate into adipocytes, but instead differentiated into well-developed large myotubes (Fig. 2b, c; Supplementary Information, Fig. S2b). In contrast, CD31$^-$CD45$^-$PDGFRα$^+$ cells had maintained PDGFRα expression, and began to express C/EBPα and PPARγ on day 4 (Fig. 2b), but they did not express myogenic markers (Supplementary Information, Fig. S2c, d). Upon adipogenic induction, over 90% of CD31$^-$CD45$^-$PDGFRα$^+$ cells differentiated into adipocytes, adopting a spherical shape, accumulating lipid and expressing C/EBPα and PPARγ (Fig. 2b, c). A clonal assay revealed that nearly 80% of clones were adipogenic (Supplementary Information, Fig. S3). After adipogenic differentiation, these cells were no longer positive for PDGFRα (Fig. 2b). PDGFRα$^+$ cell-derived adipocytes expressed much higher levels of *leptin* compared with adipocytes derived from 3T3-L1 preadipocytes, although this was lower than that of *in vivo* white adipose tissue (Fig. 2d; Supplementary Information, Fig. S4). Similar results were obtained when each muscle-derived cell population was cultured directly in adipogenic induction medium immediately after cell sorting (Supplementary Information, Fig. S5). In addition to adipogenic potential, these cells readily differentiated into osteoblastic and smooth muscle-like cells with high efficiency under specific culture conditions (Fig. 2e; Supplementary Information, Fig. S6), but scarcely differentiated into skeletal muscle cells when cultured under myogenic differentiation conditions or transplanted into regenerating muscle (data not shown; Supplementary Information, Fig. S7). The high efficiency of differentiation into three different cell types strongly suggests that muscle-derived PDGFRα$^+$ cells populations are highly enriched for mesenchymal progenitors.

Localization of PDGFRα$^+$ cells in skeletal muscle

Next, we examined the anatomical localization of PDGFRα$^+$ cells in skeletal muscle. PDGFRα$^+$ cells were localized at the interstitial space of muscle tissue, whereas satellite cells (stained with Pax7 or M-cadherin, M-cad, antibodies) were located beneath the basement membrane (Fig. 3a; Supplementary Information, Fig. S8a). These localizations again indicate that PDGFRα$^+$ cells and satellite cells represent discrete cell populations. The mesenchymal origin of the PDGFRα$^+$ cells was supported by the expression of the mesenchymal intermediate filament, Vimentin (Fig. 3b). These cells also express a known repressor of adipogenesis, Dlk1 (also known as Pref-1; Supplementary Information, Fig. S8b). As pericytes have been reported

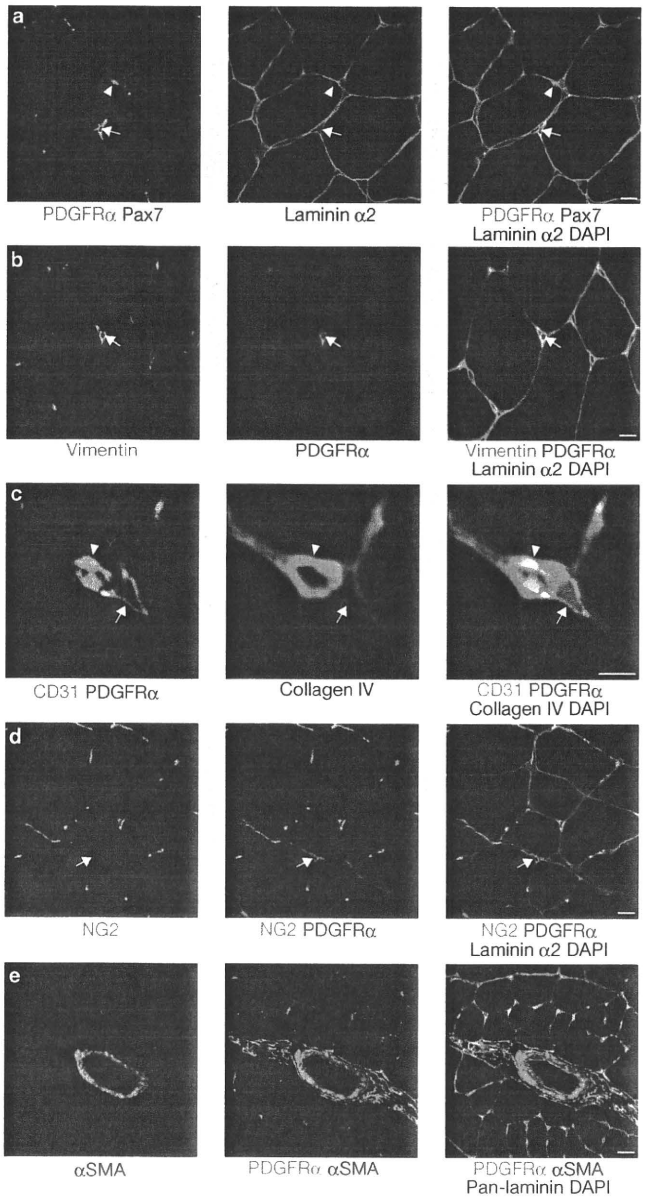

Figure 3 Localization of PDGFRα⁺ cells in adult skeletal muscle. (**a–e**) Tibialis anterior or gastrocnemius muscle sections were stained with antibodies against PDGFRα, Pax7 and laminin α2 (**a**); Vimentin, PDGFRα and laminin α2 (**b**); CD31, PDGFRα and collagen IV (**c**); NG2, PDGFRα and laminin α2 (**d**) or αSMA, PDGFRα and pan-laminin (**e**). Arrows indicate PDGFRα⁺ cells located in the interstitial space of muscle tissue. Arrowheads in **a** indicate Pax7⁺ satellite cells. Arrowheads in **c** indicate CD31⁺ capillary endothelium surrounded by basement membrane. Scale bars, 10 μm (**a**, **b**, **d**), 5 μm (**c**) and 20 μm (**e**).

to differentiate into adipocytes[20], we studied the relationship between PDGFRα⁺ cells and pericytes. The definition of pericytes is based on their anatomic location; pericytes are bound by the same basement membrane as capillary endothelial cells. PDGFRα⁺ cells were found to reside outside the capillary basement membrane (Fig. 3c) and they did not express NG2, a pericyte marker (Fig. 3d), indicating that they are distinct from pericytes. PDGFRα⁺ cells were more frequently observed in the perimysium than in the endomysium. They tended to localize circumferentially around vessels, but could be distinguished from vascular smooth muscle cells by the absence of α-smooth muscle actin (αSMA) staining (Fig. 3e).

Behaviour of PDGFRα⁺ cells during fatty degeneration of skeletal muscle

We next sought to examine the contribution of PDGFRα⁺ cells to *in vivo* fat formation in skeletal muscle. In mice, however, the occurrence of adipocytes in skeletal muscle is rare, even in pathologic mouse models such as *mdx*, DMD or obese mice. We therefore used a muscle injury model induced by injection with glycerol, which has been reported to induce destabilization of the cytoplasmic membrane followed by cell death, and eventually results in fatty degeneration of the injected muscle[21]. This model has been used to evaluate the efficacy of gene therapy for muscular disorders[21]. When glycerol was injected into the tibialis anterior muscle of C57BL/6 mice, we confirmed that muscle fibre disruption was followed by the development of adipocytes at ~7 days after injection, and a subsequent increase in fatty and fibrous connective tissue particularly in the peripheral regions of injected muscle on day 14 (Fig. 4a). Adipose cells then gradually decreased in number, but could be observed at least 1 month after injury (data not shown). We examined the behaviour of endogenous PDGFRα⁺ cells during this degeneration process. Many proliferating PDGFRα⁺ cells were observed in the interstitial space 4 days after injury (Fig. 4b). However, we could not detect expression of PDGFRα in adipocytes that had arisen in muscle on day 7 (Fig. 4c).

Only the PDGFRα⁺ population can differentiate into adipocytes in glycerol-injected fatty degenerating muscle

Given that purified PDGFRα⁺ cells lost PDGFRα expression after adipogenic differentiation *in vitro*, it was assumed that interstitial PDGFRα⁺ cells proliferate and then differentiate into adipocytes while downregulating PDGFRα. To confirm this, we transplanted cells isolated from muscles of GFP transgenic (Tg) mice into tibialis anterior muscles of wild type mice that had been injected with glycerol. Three freshly isolated cell populations, a mixed population of CD31⁺ and CD45⁺ cells, CD31⁻CD45⁻PDGFRα⁻ cells and CD31⁻CD45⁻PDGFRα⁺ cells, were transplanted immediately after cell sorting (Fig. 5a). Pax7 expression revealed by cytospin was detected only in CD31⁻CD45⁻PDGFRα⁻ cells, indicating that satellite cells were sorted in this population (data not shown). At day 14, few GFP⁺ cells were observed in muscles that had been injected with the mixed population of CD31⁺ and CD45⁺ cells (Fig. 5b). In CD31⁻CD45⁻PDGFRα⁻ cell- or CD31⁻CD45⁻PDGFRα⁺ cell-transplanted muscles, numerous GFP⁺ cells were detected (Fig. 5b). The expression of myosin heavy chain (MyHC) indicated that CD31⁻CD45⁻PDGFRα⁻ cells differentiated into myofibres (Fig. 5c). Differentiation of transplanted CD31⁻CD45⁻PDGFRα⁺ cells into mature adipocytes was confirmed by the expression of both C/EBPα and PPARγ, and the presence of a single large lipid vacuole (Fig. 5d). Quantitative analysis revealed that the myogenic potential was found exclusively in the CD31⁻CD45⁻PDGFRα⁻ population, whereas adipocytes arose only from CD31⁻CD45⁻PDGFRα⁺ cells (Fig. 5e). These results suggest that only CD31⁻CD45⁻PDGFRα⁺ cells can differentiate into adipocytes *in vivo*. To further confirm this notion, we investigated whether bone marrow-derived cells contribute to *in vivo* adipocyte formation in skeletal muscle using bone marrow chimaeric mice. Bone marrow-derived cells did not give rise to either PDGFRα⁺ cells or to adipocytes during adipogenesis induced by glycerol injection (Supplementary Information, Fig. S9). Collectively, our data suggest that muscle-resident interstitial PDGFRα⁺ cells are the sole source of adipocytes that arise in skeletal muscle in the context of glycerol-induced fatty degeneration.

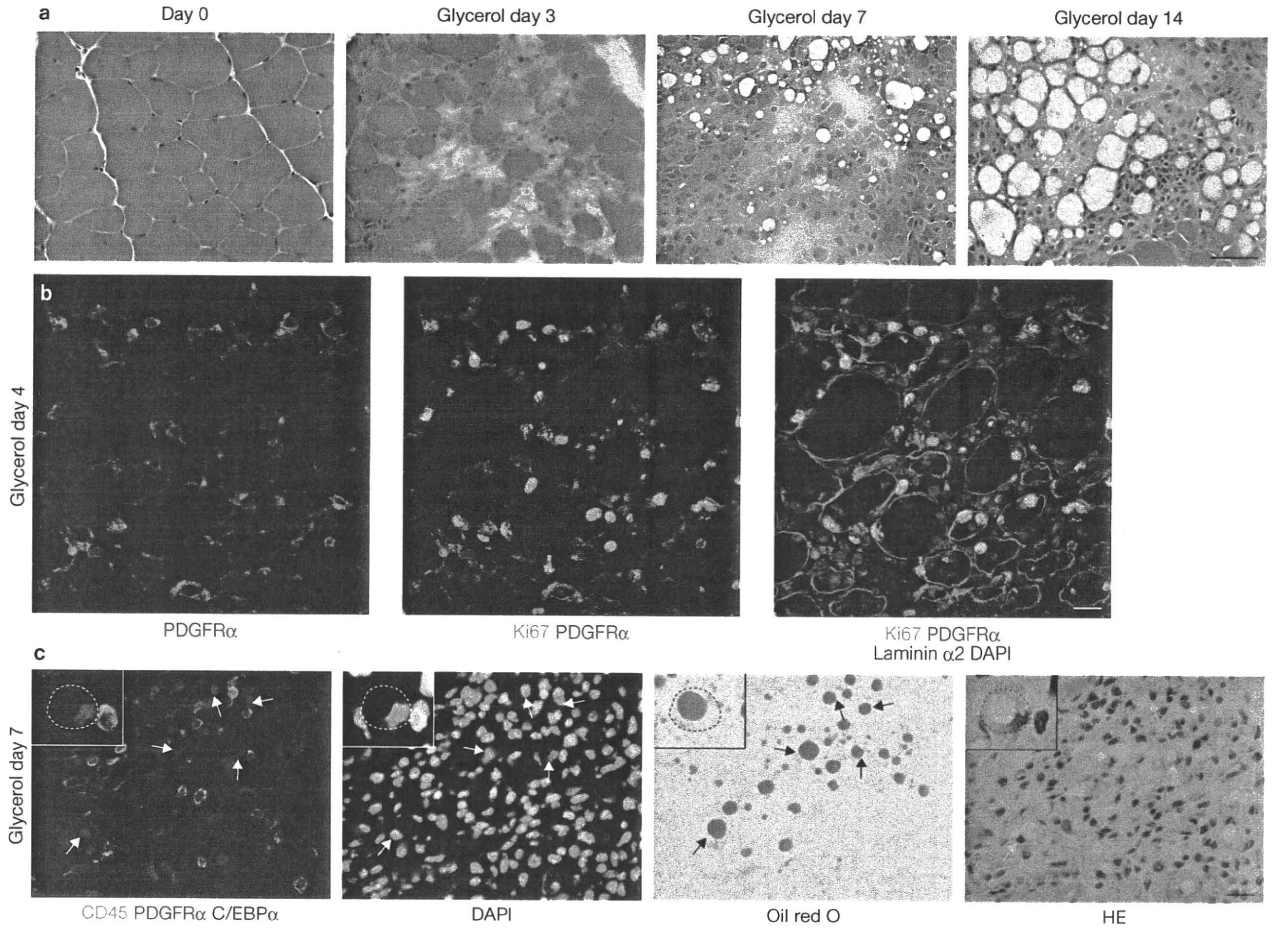

Figure 4 Behaviour of PDGFRα⁺ cells in fatty degenerating muscle. (**a**) Histological changes in skeletal muscle was analysed by hematoxylin and eosin (HE) staining during glycerol-induced fatty degeneration. Tibialis anterior muscles were injected with glycerol and, at the time points indicated, frozen muscle sections were subjected to HE staining. (**b**) Four days after glycerol injection, muscle sections were stained with anti-PDGFRα, anti-Ki67 and anti-laminin α2 antibodies. (**c**) On day 7 after glycerol injection, muscle sections were subjected to immunofluorescence staining for CD45, PDGFRα and C/EBPα, and subsequently to oil red O staining followed by HE staining. C/EBPα⁺ oil red O⁺ unilocular adipocytes were negative for CD45 and PDGFRα (arrows and insets). Scale bars, 50 μm (**a**) and 20 μm (**b**, **c**).

The fate of PDGFRα⁺ cells is largely dependent on the muscle environment

To understand how *in vivo* adipogenesis of PDGFRα⁺ cells is regulated, we used a muscle regeneration model induced by cardiotoxin (CTX) injection. In contrast to glycerol injection, CTX injection rarely induces adipocyte formation in the skeletal muscle of C57BL/6 mice. Thus, it is expected that the behaviour of PDGFRα⁺ cells in CTX-injected muscle is regulated in a manner distinct to those in muscle with a glycerol-induced injury. Intriguingly, PDGFRα⁺ cells significantly increased in number in CTX-induced regenerating muscle as well as in glycerol-injected degenerating muscle (Fig. 6a). However, the number of PDGFRα⁺ cells decreased without differentiating into adipocytes as muscle regeneration proceeded (Fig. 6a). We isolated proliferating PDGFRα⁺ cells from both CTX-injected and glycerol-injected muscles and compared their adipogenic potentials. Both were largely negative for C/EBPα immediately after isolation (Fig. 6b). Surprisingly, they showed comparable levels of adipogenic potential under adipogenic culture conditions (Fig. 6c, d). Thus, non-cell-autonomous mechanisms are likely to determine the differences between cell fate resulting from CTX injection and glycerol injection. To test this directly, we performed reciprocal transplantations between regenerating and degenerating muscles (Fig. 7a). If the adipogenic fate of PDGFRα⁺ cells is already determined at day 4 of glycerol injection, PDGFRα⁺ cells isolated from glycerol-injected muscle should form adipocytes, even in CTX-injected regenerating muscle, in a cell-autonomous manner. If the muscle environment determines PDGFRα⁺ cell adipogenic fate, PDGFRα⁺ cells isolated from CTX-injected muscle should adapt their fate to an adipocyte lineage in glycerol-injected muscle. The results demonstrate that the latter is the case. PDGFRα⁺ cells isolated from glycerol-injected muscle did not differentiate into adipocytes in CTX-injected muscle, where only a few transplanted cells were observed that were similar to endogenous PDGFRα⁺ cells (Fig. 7b, e). In contrast, PDGFRα⁺ cells isolated from CTX-injected muscle accumulated in degenerated areas and differentiated into C/EBPα⁺PPARγ⁺, lipid-laden adipocytes in glycerol-injected muscle (Fig. 7c–e). These results clearly show that the fate of PDGFRα⁺ cells is largely regulated by the surrounding muscle environment.

Muscle fibres have a strong inhibitory effect on the adipogenesis of PDGFRα⁺ cells

Our results indicate that the muscle environment after the fourth day of CTX injection has an inhibitory effect on adipogenesis of PDGFRα⁺ cells,

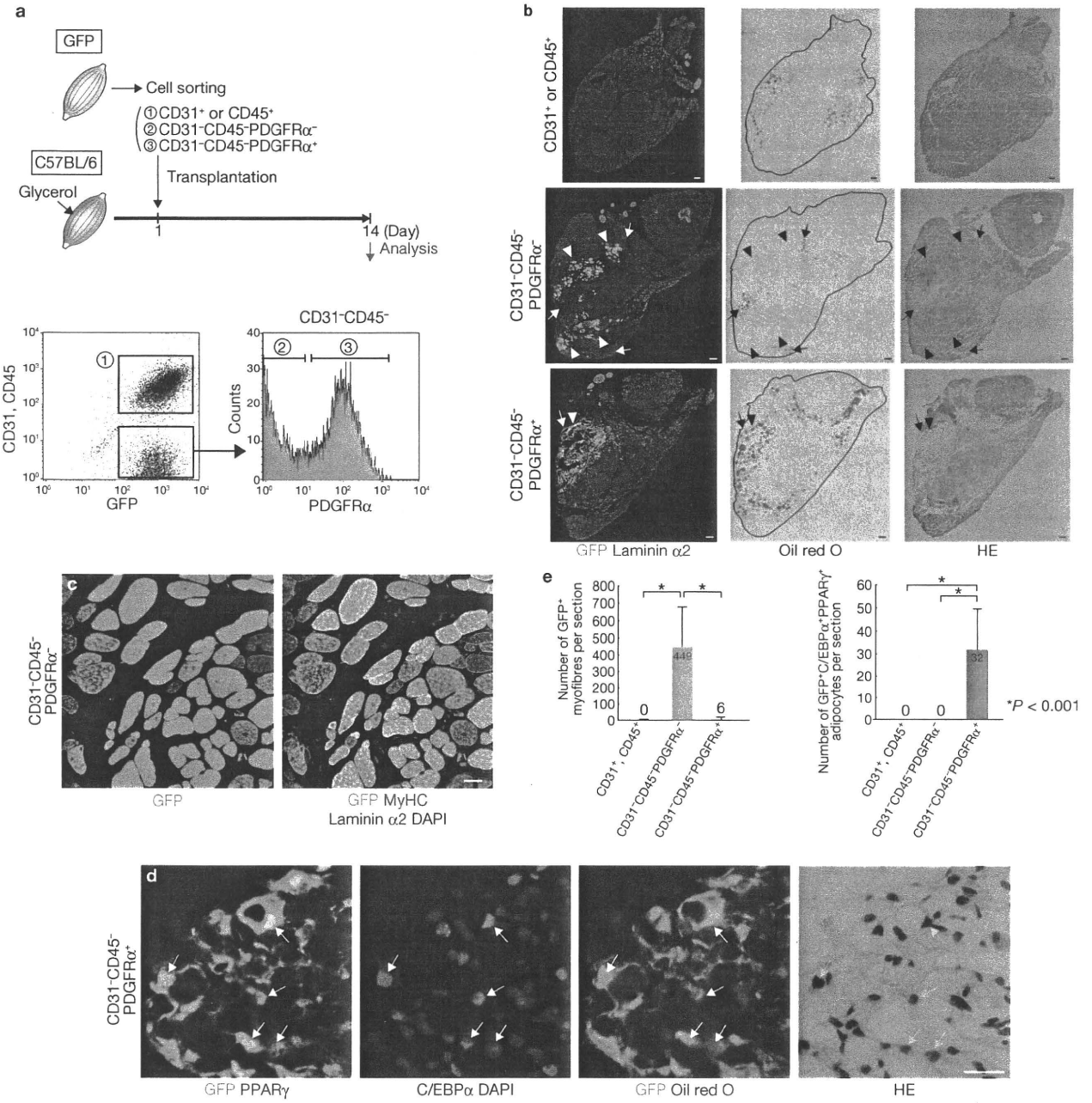

Figure 5 Only PDGFRα+ cells differentiate into adipocytes after transplantation into glycerol-injured muscle. (**a**) Transplantation procedures. (**b**) On day 14 after glycerol injection, transplanted muscle sections were subjected to immunofluorescence staining for GFP and laminin α2, and subsequently to oil red O staining followed by hematoxylin and eosin (HE) staining. Arrowheads indicate GFP+ area. Arrows indicate oil red O+ fatty degenerated area. (**c**) CD31-CD45-PDGFRα- cell-transplanted muscles were analysed for expression of GFP, MyHC and laminin α2. (**d**) Sections of CD31-CD45-PDGFRα+ cell-transplanted muscles were subjected to immunofluorescence staining for GFP, C/EBPα and PPARγ, and subsequently to oil red O staining followed by HE staining. Arrows indicate GFP+C/EBPα+PPARγ+oil red O+ unilocular adipocytes. (**e**) Quantitative analysis of transplantation experiments. Error bars indicate the mean ± s.d., $n = 6$ in each group. Scale bars, 100 μm (**b**) and 20 μm (**c**, **d**).

whereas the muscle environment after the fourth day of glycerol injection facilitates adipogenesis. Active differentiation of myogenic cells and new myofibre formation occurs after day 4 of CTX injection[22]. Therefore, we examined myogenic differentiation in both CTX and glycerol models. Administration of 5-ethynyl-2′-deoxyuridine (EdU) in combination with embryonic MyHC (eMyHC) staining was performed to analyse *de novo* myofibre formation. Five days after injury, much higher numbers of eMyHC+EdU+ new myofibres were observed in CTX-injected muscles compared with glycerol-injected muscles (Fig. 8a, b, e). Myogenin staining further revealed that muscle regeneration was severely compromised in glycerol-injected muscles (Fig. 8c–e). At this time point, PDGFRα+ cells showing an elongated spindle shape were distributed in the narrow space between regenerating myofibres in CTX-injected muscles, whereas many PDGFRα+ cells were observed in the extended interstitial space between degenerating myofibres and showed an enlarged rounded morphology in glycerol-injected muscles (Fig. 8c, d). This impairment

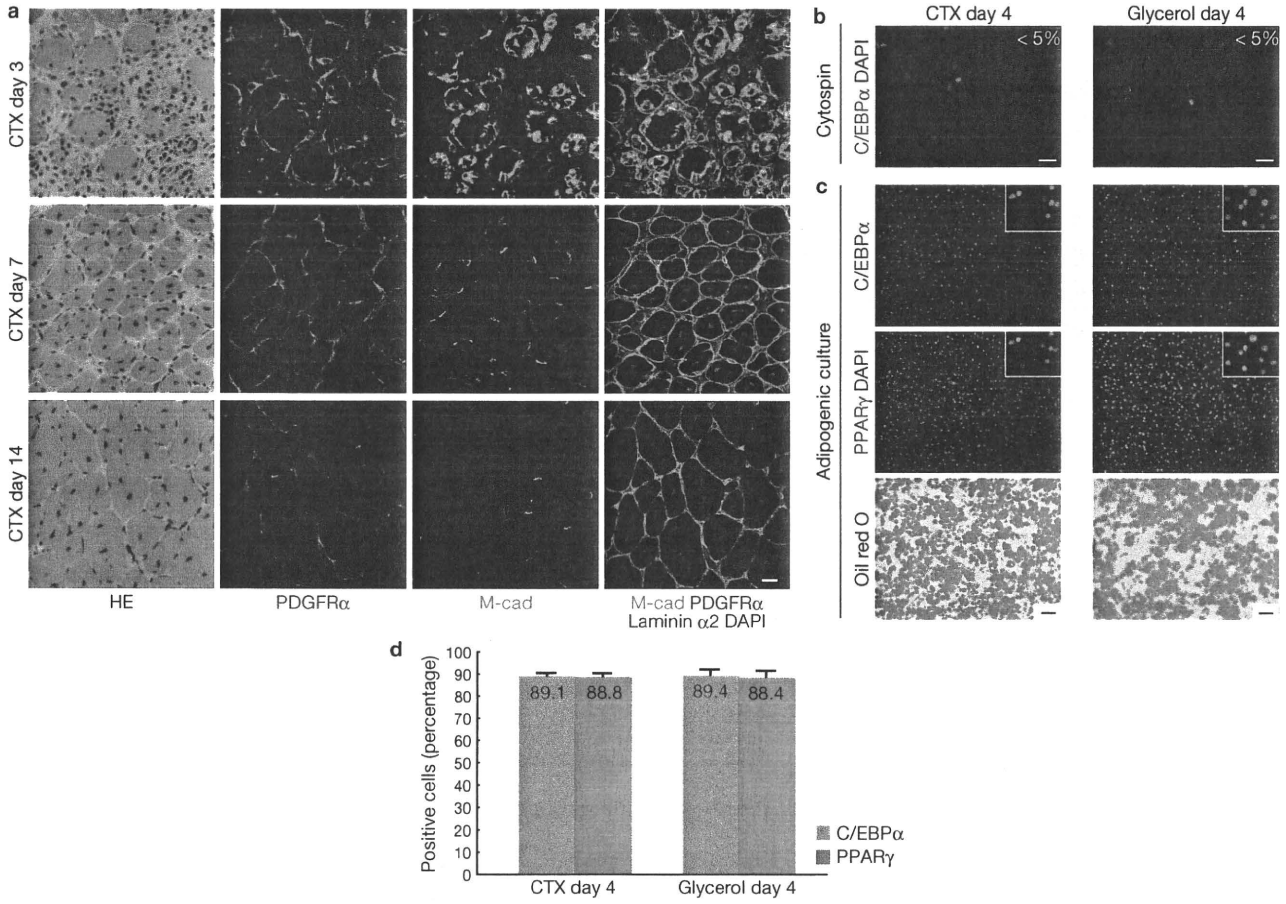

Figure 6 The behaviour of PDGFRα⁺ cells during CTX-induced muscle regeneration and adipogenic potentials of PDGFRα⁺ cells isolated from regenerating or degenerating muscle. (**a**) At the indicated time points after CTX injection, muscle sections were subjected to immunofluorescence staining for M-cadherin (M-cad), PDGFRα and laminin α2 before hematoxylin and eosin (HE) staining. (**b**) Four days after CTX or glycerol injection, CD31⁻CD45⁻PDGFRα⁺ cells were isolated from treated muscles and subjected to cytospin and then analysed for C/EBPα expression. The values in the top panels represent the percentages of positive cells. (**c**) CD31⁻CD45⁻PDGFRα⁺ cells isolated from CTX or glycerol-injected muscles were cultured under adipogenic conditions. Adipogenic differentiation was revealed by immunofluorescence staining for C/EBPα and PPARγ or by oil red O staining. (**d**) Adipogenic differentiation was evaluated by quantifying the percentages of C/EBPα- and PPARγ-positive cells. Error bars indicate the mean ± s.d., $n = 15$ fields pulled out from three independent experiments. Scale bars, 20 μm (**a**) 30 μm (**b**) and 50 μm (**c**).

in the regeneration of glycerol-injected muscles could be attributed to impaired proliferation of Pax7⁺ myogenic progenitors at an earlier stage (Supplementary Information, Fig. S10). At day 14, in the CTX model, regenerated myofibres with central nuclei were located throughout the tibialis anterior muscles and adipocytes were rare (Fig. 8f–f′′′, h). In contrast, glycerol-injected muscle had fewer regenerated myofibres, and ectopic adipocytes as well as necrotic fibres occupied a considerable area of the muscles (Fig. 8g–g′′′, h). These results suggest that interaction between regenerating myofibres and PDGFRα⁺ cells may be important for the inhibition of ectopic fat formation. To examine the effect of interaction between myofibres and PDGFRα⁺ cells, GFP⁺PDGFRα⁺ cells were co-cultured with wild-type satellite cells. In marked contrast to a single culture, adipogenic differentiation of PDGFRα⁺ cells was dramatically inhibited in co-culture (Fig. 8i, j). GFP⁺ cells occupied spaces between GFP⁻ satellite cell-derived myotubes, and most of them were negative for adipogenic markers (Fig. 8j). GFP⁺ adipocytes expressing C/EBPα and PPARγ were only rarely observed in co-culture (Fig. 8j, l). These results suggest that satellite cell-derived muscle fibres generate factors that strongly inhibit adipogenic differentiation of PDGFRα⁺ cells. To investigate whether such factors are produced in soluble forms, we generated conditioned cultures. Satellite cells were treated with adipogenic induction medium for 1 day. During this conditioning period, satellite cells rapidly differentiated and formed large myotubes (data not shown). Therefore, soluble factors produced by differentiating myoblasts or differentiated myotubes should have been present in the culture supernatant. When this conditioned medium was applied to the solo culture of PDGFRα⁺ cells, we could not see any inhibitory effects on adipogenic differentiation (Fig. 8k, l). In a transwell co-culture where PDGFRα⁺ cells and satellite cells were separated by a culture insert with 1.0-μm pore, inhibition of PDGFRα⁺ cell-dependent adipogenesis was not observed (data not shown). Taken together, our results suggest that satellite cell-derived muscle fibres exert an inhibitory effect on the adipogenesis of PDGFRα⁺ cells by directly interacting with them.

DISCUSSION

In this study, we identified mesenchymal progenitors in skeletal muscle using PDGFRα as a marker. PDGFRα is known to be expressed in mesenchymal cells. Particularly strong expression of PDGFRα has been observed in subtypes of mesenchymal progenitor cells and oligodendrocyte progenitors,

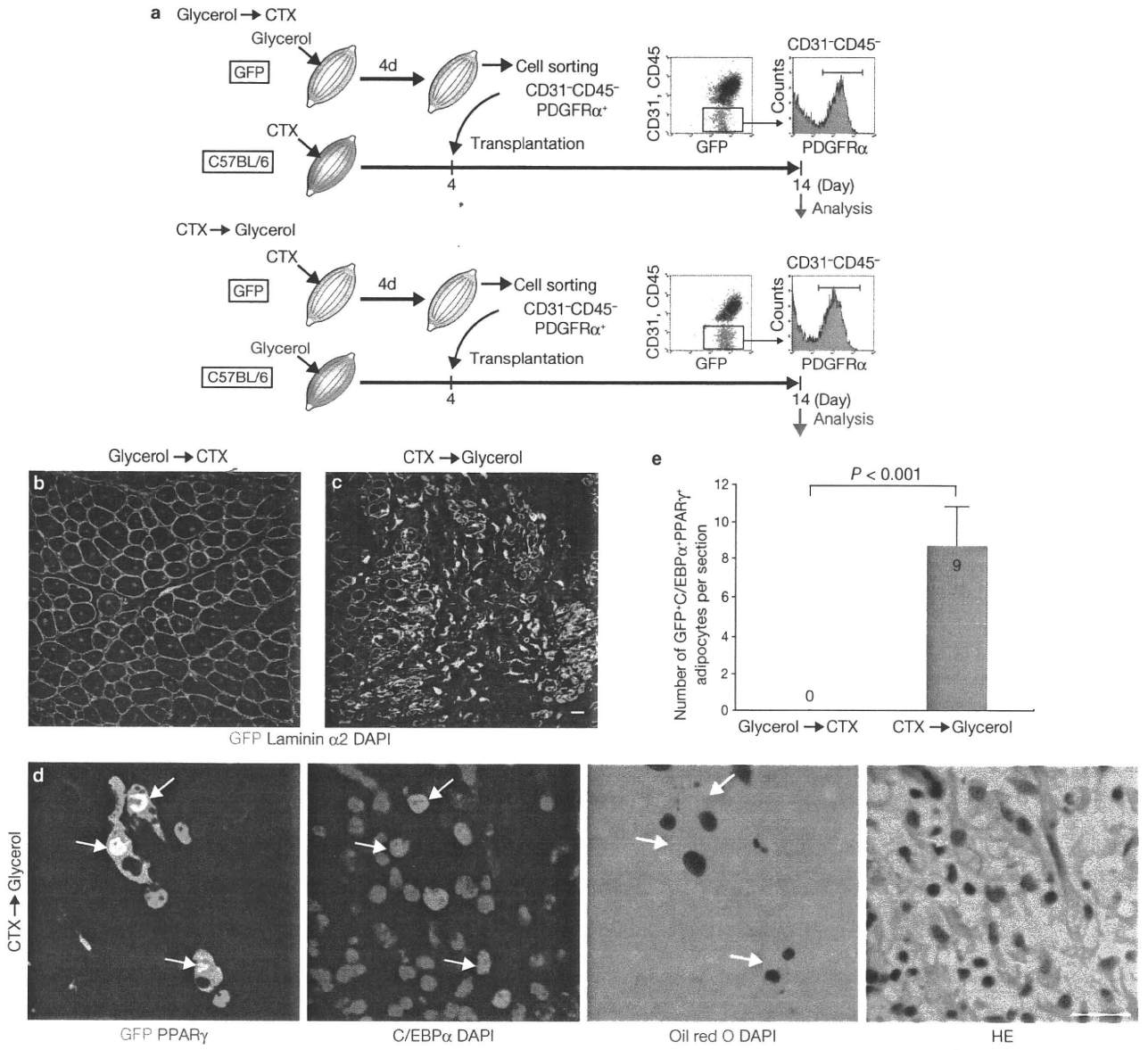

Figure 7 The fate of PDGFRα⁺ cells is largely dependent on the muscle environment. (**a**) Reciprocal transplantation procedures. (**b**, **c**) Two weeks after transplantation, the transplanted muscles were analysed for expression of GFP and laminin α2. (**d**) Adipogenic differentiation of transplanted cells was revealed by immunofluorescence staining for GFP, C/EBPα and PPARγ, and subsequent oil red O staining followed by hematoxylin and eosin (HE) staining. Arrows indicate GFP⁺C/EBPα⁺PPARγ⁺ oil red O⁺ unilocular adipocytes. (**e**) Quantitative analysis of reciprocal transplantation experiments. Error bar indicates the mean ± s.d., $n = 6$ in each group.

and PDGF-A–PDGFRα signalling appears to regulate a broad range of progenitor cells in several developmental processes[23]. During somitogenesis, PDGFRα is initially expressed throughout the undifferentiated somite and later becomes progressively restricted to the sclerotome and to a lesser extent the dermatome, but its expression disappears in the myotome as differentiation of the somite proceeds[24]. In a previous study, paraxial mesodermal progenitors were isolated from *Pax3*-induced embryoid bodies using PDGFRα as a positive selection marker, however, this receptor was downregulated in the derivative myogenic cells[25]. Thus, it seems that early mesodermal progenitors lose PDGFRα expression when they differentiate into the myogenic lineage. Recently, PDGFRα⁺ cells have been isolated from mouse bone marrow and characterized as a population highly enriched for MSCs[26–28]. Both PDGFRα and PDGFRβ are expressed in MSCs, but MSCs have a higher cell surface PDGFRα:PDGFRβ ratio than the differentiated cell type, and abundant PDGFRα appears to be a characteristic of undifferentiated MSCs[29]. Similarly, we observed downregulation of PDGFRα after adipogenic differentiation of muscle mesenchymal progenitors. Taken together, these results indicate that PDGFRα is an excellent marker for stem or progenitor cells of mesenchymal lineages.

Adipocyte progenitor cells have been previously identified in white adipose tissue using a FACS-based cell isolation method[30]. Interestingly, the white adipose tissue progenitors and mesenchymal progenitors in muscle reported here have a similar cell-surface phenotype (CD31⁻CD45⁻CD29⁺CD34⁺Sca-1⁺), raising the possibility that progenitors with common cell-surface phenotypes may be isolated from diverse tissues.

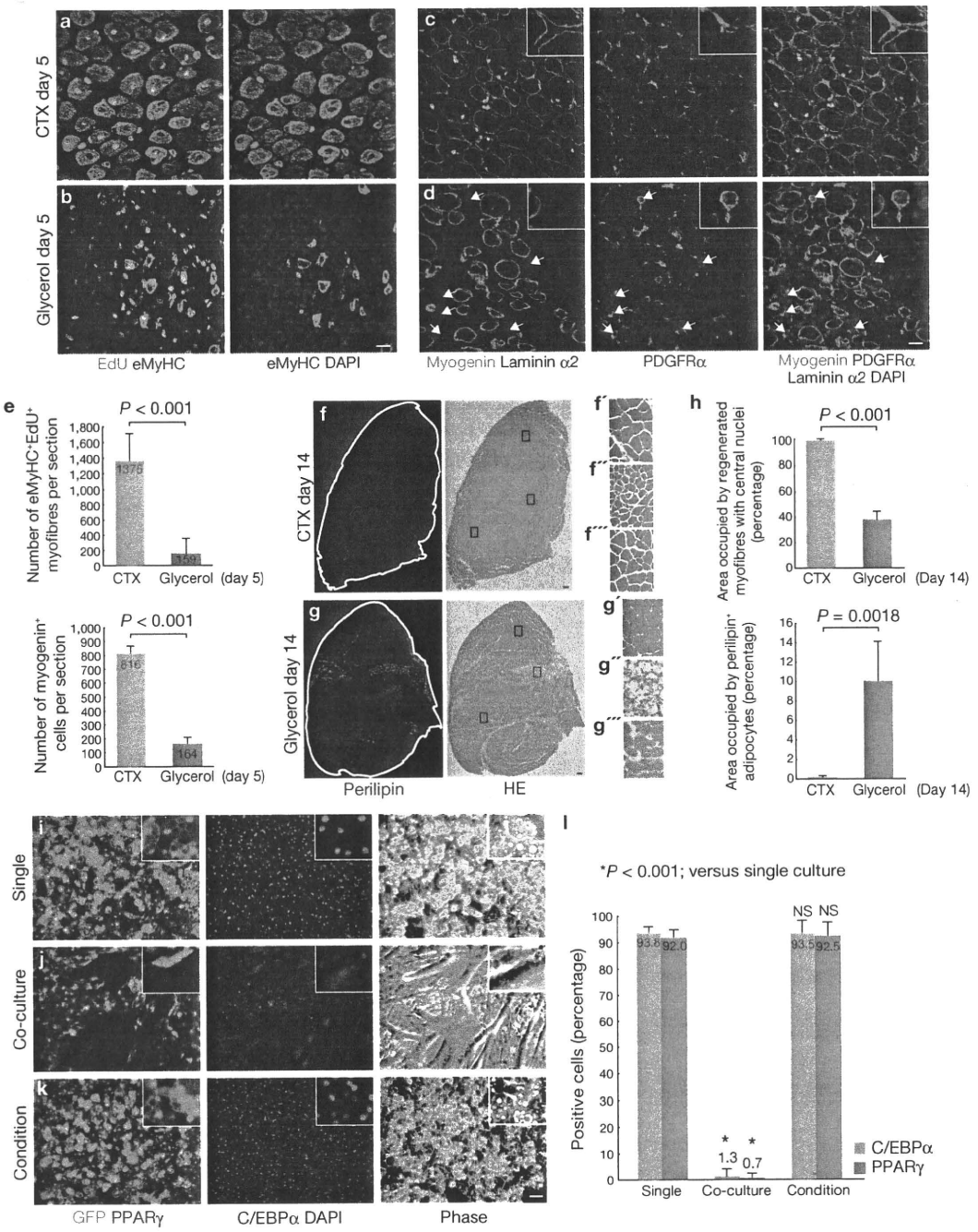

Figure 8 Satellite cell-derived myofibres inhibit adipogenic differentiation of PDGFRα⁺ cells. (**a**, **b**) EdU was administered 2, 3 and 4 days after CTX (**a**) or glycerol (**b**) injection. Five days after injury, muscle sections were subjected to eMyHC staining followed by EdU detection. (**c**, **d**) Expression of myogenin, PDGFRα and laminin α2 at day 5 after CTX (**c**) or glycerol (**d**) injection. Arrows indicate PDGFRα⁺ cells that lost physical interaction with myofibres and showed a morphological change in glycerol-injected muscle. Insets show high magnification images. (**e**) Quantitative analysis of eMyHC⁺EdU⁺ myofibres ($n = 6$ in each group) and myogenin⁺ cells ($n = 4$ in each group). Error bars indicate the mean ± s.d. (**f**–**g‴**) Muscle sections were subjected to perilipin staining followed by hematoxylin and eosin (HE) staining 14 days after injury. High magnification images of rectangular regions in **f** and **g** are shown in **f′**–**f‴** and **g′**–**g‴**, respectively. Glycerol-injected muscle had large areas occupied by adipocytes (**g″**) or necrotic fibres (**g‴**). (**h**) Quantitative analysis of regenerated area and fatty degenerated area. Error bars indicate mean ± s.d., $n = 4$ in the CTX group and $n = 5$ in the glycerol group. (**i**–**k**) CD31⁻CD45⁻SM/C-2.6⁻PDGFRα⁺ cells isolated from GFP Tg mice were cultured with or without wild-type CD31⁻CD45⁻SM/C-2.6⁺ cells. Cultures were treated with adipogenic medium or satellite cell-conditioned medium. Adipogenic differentiation was revealed by immunofluorescence staining for GFP, C/EBPα and PPARγ. (**l**) Adipogenic differentiation was evaluated by quantifying the percentages of C/EBPα- and PPARγ-positive GFP⁺ cells. Error bars indicate the mean ± s.d., $n = 15$ (single and condition cultures) or 20 (co-cultures) fields pulled from three independent experiments. NS, not significant. Scale bars, 20 μm (**a**–**d**), 100 μm (**f**, **g**) and 50 μm (**i**–**k**).

The physiological roles of PDGFRα⁺ mesenchymal progenitors remain to be elucidated. However, they may provide a supporting function for the muscle, as they encircle the sheath of muscle basement membrane in which satellite cells undergo active myogenesis during muscle regeneration (Fig. 6a). Interestingly, CD90⁺ fibroblast-like cells in skeletal muscle produce the muscle basement membrane component

laminin α2 (ref. 31), and PDGFRα$^+$ and CD90$^+$ cells are nearly identical (Supplementary Information, Fig. S1a). Thus, PDGFRα$^+$ cells may have positive roles in muscle regeneration in part by producing basement membrane that functions as a scaffold for efficient myogenesis.

This study highlights the importance of PDGFRα$^+$ mesenchymal progenitors in the context of ectopic fat formation in skeletal muscle. In obesity and various myopathies, fat accumulation is known to be more conspicuous in perimysium, particularly in perivascular space[2,5], where PDGFRα$^+$ cells are commonly observed (Fig. 3e). One of the most intriguing results of our study is that factor(s) from satellite cell-derived myofibres strongly inhibited adipogenesis of PDGFRα$^+$ cells. Thus, it seems that the balance between satellite cell-dependent myogenesis and PDGFRα$^+$ cell-dependent adipogenesis, rather than multipotency of satellite cells, has a considerable impact on muscle homeostasis. As ectopic adipocytes usually arise under disease conditions where there has been destruction of muscle fibres without efficient regeneration[3], the model in which myofibres themselves have an inhibitory effect on the adipogenesis of PDGFRα$^+$ cells makes sense. However, there are cases where our model would not apply, including obesity and type II diabetes[4,5], as there is no apparent muscle destruction in such diseases. In these conditions, systemic factors may have a role in the regulation of the adipogenesis of PDGFRα$^+$ cells. In fact, we used high glucose medium containing several pro-adipogenic inducers for *in vitro* adipogenic differentiation. Additional experiments revealed that IBMX and dexamethasone are unnecessary, but insulin is required for efficient adipogenic differentiation of PDGFRα$^+$ cells (data not shown). Furthermore, a high glucose condition is reported to enhance adipogenic differentiation of muscle-derived cells[32]. Thus, it is possible that systemic factors such as hormonal level or nutrition status may exert a stimulatory influence on the adipogenesis of PDGFRα$^+$ cells. Overall, the fate of PDGFRα$^+$ cells can be influenced by several aspects of the environment, and the balance between positive and negative factors may determine the final outcome.

In conclusion, we report the identification of PDGFRα$^+$ mesenchymal progenitors that contribute to adipogenesis in skeletal muscle, and demonstrate a possible role for myofibres in regulating the fate of PDGFRα$^+$ cells. We suggest that these cells are responsible for ectopic fat cell formation within skeletal muscle in pathological conditions such as DMD, denervation, obesity and ageing-related sarcopenia. Targeting PDGFRα$^+$ mesenchymal progenitors may open new opportunities for designing therapeutic strategies to treat muscle diseases. □

METHODS

Methods and any associated references are available in the online version of the paper at http://www.nature.com/naturecellbiology/.

Note: Supplementary Information is available on the Nature Cell Biology website.

ACKNOWLEDGEMENTS

We thank S. Miura, M. Nakatani and T. Sato for technical assistance, F. Rossi for providing DyLight 649-conjugated rat anti-integrin α7, A. Miyajima for providing a rat anti-Dlk1 antibody and N. Hashimoto for providing a rabbit anti-myogenin antibody. This work was supported by JSPS KAKENHI (18890216; to A.U.), MEXT KAKENHI (21790884; to A.U.), a research grant (H20-018) on psychiatric and neurological diseases and mental health and a research grant (20B-13) for nervous and mental disorders from the Ministry of Health, Labour and Welfare.

AUTHOR CONTRIBUTIONS

A.U. was responsible for designing and performing the experiments, analysing the data and writing the manuscript; S.F. performed BM-transplantation and provided reagents; A.U. performed FACS experiment with help from N.Y.; S.T. provided reagents and materials and A.U. and K.T. coordinated the whole project.

COMPETING FINANCIAL INTERESTS

The authors declare no competing financial interests.

Published online at http://www.nature.com/naturecellbiology/.
Reprints and permissions information is available online at http://npg.nature.com/reprintsandpermissions/.

1. Bischoff, R. Satellite and stem cells in muscle regeneration, in *Myology*, Vol. 1, Edn. 3. (eds. A. G. Engel & C. Franzini-Armstrong) 66–86 (McGraw-Hill, New York; 2004).
2. Banker, B. Q. & Engel, A. G. Basic reactions of muscle, in *Myology*, Vol. 1, Edn. 3. (eds. A. G. Engel & C. Franzini-Armstrong) 691–747 (McGraw-Hill, New York; 2004).
3. Carpenter, S. & Karpati, G. Cells and structures other than skeletal muscle fibers, in *Pathology of skeletal muscle*, Edn. 2 314–369 (Oxford, New York; 2001).
4. Goodpaster, B. H. & Wolf, D. Skeletal muscle lipid accumulation in obesity, insulin resistance, and type 2 diabetes. *Pediatr. Diabetes* **5,** 219–226 (2004).
5. Greco, A. V. *et al.* Insulin resistance in morbid obesity: reversal with intramyocellular fat depletion. *Diabetes* **51,** 144–151 (2002).
6. Visser, M. *et al.* Muscle mass, muscle strength, and muscle fat infiltration as predictors of incident mobility limitations in well-functioning older persons. *J. Gerontol. A Biol. Sci. Med. Sci.* **60,** 324–333 (2005).
7. Rosen, E. D. & Macdougald, O. A. Adipocyte differentiation from the inside out. *Nature Rev. Mol. Cell Biol.* **7,** 885–896 (2006).
8. Gregoire, F. M., Smas, C. M. & Sul, H. S. Understanding adipocyte differentiation. *Physiol. Rev.* **78,** 783–809 (1998).
9. Linhart, H. G. *et al.* C/EBPα is required for differentiation of white, but not brown, adipose tissue. *Proc. Natl Acad. Sci. USA* **98,** 12532–12537 (2001).
10. Tontonoz, P., Hu, E. & Spiegelman, B. M. Stimulation of adipogenesis in fibroblasts by PPARγ 2, a lipid-activated transcription factor. *Cell* **79,** 1147–1156 (1994).
11. Asakura, A., Komaki, M. & Rudnicki, M. Muscle satellite cells are multipotential stem cells that exhibit myogenic, osteogenic, and adipogenic differentiation. *Differentiation* **68,** 245–253 (2001).
12. Shefer, G., Wleklinski-Lee, M. & Yablonka-Reuveni, Z. Skeletal muscle satellite cells can spontaneously enter an alternative mesenchymal pathway. *J. Cell Sci.* **117,** 5393–5404 (2004).
13. Uezumi, A. *et al.* Functional heterogeneity of side population cells in skeletal muscle. *Biochem. Biophys. Res. Commun.* **341,** 864–873 (2006).
14. Young, H. E. *et al.* Human reserve pluripotent mesenchymal stem cells are present in the connective tissues of skeletal muscle and dermis derived from fetal, adult, and geriatric donors. *Anat. Rec.* **264,** 51–62 (2001).
15. da Silva Meirelles, L., Chagastelles, P. C. & Nardi, N. B. Mesenchymal stem cells reside in virtually all post-natal organs and tissues. *J. Cell Sci.* **119,** 2204–2213 (2006).
16. Fukada, S. *et al.* Purification and cell-surface marker characterization of quiescent satellite cells from murine skeletal muscle by a novel monoclonal antibody. *Exp. Cell Res.* **296,** 245–255 (2004).
17. Orr-Urtreger, A., Bedford, M. T., Do, M. S., Eisenbach, L. & Lonai, P. Developmental expression of the α receptor for platelet-derived growth factor, which is deleted in the embryonic lethal Patch mutation. *Development* **115,** 289–303 (1992).
18. Shinbrot, E., Peters, K. G. & Williams, L. T. Expression of the platelet-derived growth factor β receptor during organogenesis and tissue differentiation in the mouse embryo. *Dev. Dyn.* **199,** 169–175 (1994).
19. De Palma, M. *et al.* Tie2 identifies a hematopoietic lineage of proangiogenic monocytes required for tumor vessel formation and a mesenchymal population of pericyte progenitors. *Cancer Cell* **8,** 211–226 (2005).
20. Farrington-Rock, C. *et al.* Chondrogenic and adipogenic potential of microvascular pericytes. *Circulation* **110,** 2226–2232 (2004).
21. Arsic, N. *et al.* Vascular endothelial growth factor stimulates skeletal muscle regeneration *in vivo*. *Mol. Ther.* **10,** 844–854 (2004).
22. Hawke, T. J. & Garry, D. J. Myogenic satellite cells: physiology to molecular biology. *J. Appl. Physiol.* **91,** 534–551 (2001).
23. Andrae, J., Gallini, R. & Betsholtz, C. Role of platelet-derived growth factors in physiology and medicine. *Genes Dev.* **22,** 1276–1312 (2008).
24. Orr-Urtreger, A. & Lonai, P. Platelet-derived growth factor-A and its receptor are expressed in separate, but adjacent cell layers of the mouse embryo. *Development* **115,** 1045–1058 (1992).
25. Darabi, R. *et al.* Functional skeletal muscle regeneration from differentiating embryonic stem cells. *Nature Med.* **14,** 134–143 (2008).
26. Takashima, Y. *et al.* Neuroepithelial cells supply an initial transient wave of MSC differentiation. *Cell* **129,** 1377–1388 (2007).
27. Morikawa, S. *et al.* Development of mesenchymal stem cells partially originate from the neural crest. *Biochem. Biophys. Res. Commun.* **379,** 1114–1119 (2009).
28. Morikawa, S. *et al.* Prospective identification, isolation, and systemic transplantation of multipotent mesenchymal stem cells in murine bone marrow. *J. Exp. Med.* **206,** 2483–2496 (2009).
29. Ball, S. G., Shuttleworth, C. A. & Kielty, C. M. Platelet-derived growth factor receptor-is a key determinant of smooth muscle α-actin filaments in bone marrow-derived mesenchymal stem cells. *Int. J. Biochem. Cell Biol.* **39,** 379–391 (2007).
30. Rodeheffer, M. S., Birsoy, K. & Friedman, J. M. Identification of white adipocyte progenitor cells *in vivo*. *Cell* **135,** 240–249 (2008).
31. Fukada, S. *et al.* CD90-positive cells, an additional cell population, produce laminin α2 upon transplantation to dy(3k)/dy(3k) mice. *Exp. Cell Res.* **314,** 193–203 (2008).
32. Aguiari, P. *et al.* High glucose induces adipogenic differentiation of muscle-derived stem cells. *Proc. Natl Acad. Sci. USA* **105,** 1226–1231 (2008).

Development, Growth & Differentiation
The Japanese Society of Developmental Biologists

Develop. Growth Differ. (2010) **52**, 693–699 doi: 10.1111/j.1440-169X.2010.01206.x

Original Article

Delivery of small interfering RNA with a synthetic collagen poly(Pro-Hyp-Gly) for gene silencing *in vitro* and *in vivo*

Taro Adachi,[1] Emi Kawakami,[2] Naozumi Ishimaru,[3] Takahiro Ochiya,[4] Yoshio Hayashi,[3] Hideyo Ohuchi,[1] Masao Tanihara,[5] Eiji Tanaka[2] and Sumihare Noji[1]*

[1]*Department of Life Systems, Institute of Technology and Science, The University of Tokushima Graduate School, 2-1 Minami-Jyosanjima;* [2]*Department of Orthodontics and Dentofacial Orthopedics, Institute of Health Bioscience, The University of Tokushima Graduate School, 3-18-15 Kuramotocho;* [3]*Department of Oral Molecular Pathology, Institute of Health Biosciences, University of Tokushima Graduate School, Kuramotocho, Tokushima 770-8504;* [4]*National Cancer Center Research Institute, Chuo-ku, Tokyo 104-0045;* [5]*Graduate School of Materials Science, Nara Institute of Science and Technology, Ikoma, Nara 630-0192, Japan*

Silencing gene expression by small interfering RNAs (siRNAs) has become a powerful tool for the genetic analysis of many animals. However, the rapid degradation of siRNA and the limited duration of its action *in vivo* have called for an efficient delivery technology. Here, we describe that siRNA complexed with a synthetic collagen poly(Pro-Hyp-Gly) (SYCOL) is resistant to nucleases and is efficiently transferred into cells *in vitro* and *in vivo*, thereby allowing long-term gene silencing *in vivo*. We found that the SYCOL-mediated local application of siRNA targeting *myostatin*, coding a negative regulator of skeletal muscle growth, in mouse skeletal muscles, caused a marked increase in the muscle mass within a few weeks after application. Furthermore, *in vivo* administration of an anti-luciferase siRNA/SYCOL complex partially reduced luciferase expression in xenografted tumors *in vivo*. These results indicate a SYCOL-based non-viral delivery method could be a reliable simple approach to knockdown gene expression by RNAi *in vivo* as well as *in vitro*.

Key words: delivery, myostatin, RNAi, siRNA, synthetic collagen.

Introduction

Induction of RNA interference (RNAi) by small interfering RNA (siRNA) is a useful method for knocking down molecular targets specifically (Tiemann & Rossi 2009). However, there exists a delivery problem: The siRNA alone can not be transported across cell membranes to the cytosol, due to its large molecular weight (~13 kDa) and strong anionic charge of the siRNA phosphodiester backbone (~40 negative phosphate charges) (Behlke 2006). Consequently, carrier development for siRNA delivery has been one of the most important problems to solve before siRNA can achieve widespread basic and clinical use. Multiple nonviral delivery systems have been introduced so far in order to deliver siRNA efficiently including chemical modification of siRNA, cationic polymers, cationic lipids, cell-penetrating peptide, and targeted delivery (for review, see (Kim & Kim 2009; Kim *et al.* 2009)). Several promising carriers with low toxicity and increased specificity for target cells or tissues have emerged for siRNA-based experiments (Kim *et al.* 2009).

One of the promising carriers for effective gene silencing *in vitro* and *in vivo* is Atelocollagen (ATCOL) (Minakuchi *et al.* 2004), which is a highly purified pepsin-treated type I collagen from calf dermis. ATCOL obtained by pepsin treatment is low in immunogenicity because it is free from telopeptides (Stenzel *et al.* 1974), and it has been used clinically for a wide range of purposes, including wound-healing, vessel prosthesis and also as a bone cartilage substitute and hemostatic agent (Ochiya *et al.* 2001). We previously showed that when siRNA targeting *myostatin*, coding a negative regulator of skeletal muscle growth, was introduced locally or systemically into mouse skeletal

*Author to whom all correspondence should be addressed.
Email: noji@bio.tokushima-u.ac.jp
Received 3 April 2010; revised 13 June 2010; accepted 25 June 2010.

muscles with ATCOL, the muscle mass markedly increased within a few weeks after application (Kinouchi *et al.* 2008). However, delivery mechanisms of siRNA by ATCOL in cells have not been elucidated yet.

In the present study, to find collagen structures essential for siRNA delivery, we examined whether a simple synthetic collagen (SYCOL) functions similarly as ATCOL. As a simple collagen-model peptide, we used a synthesized collagen poly(Pro-Hyp-Gly) which forms a stable triple-helical structure (Kishimoto *et al.* 2005), because Pro-Hyp-Gly is a characteristic amino acid sequence found in fibrous collagens. We suspended siRNA in a solution of poly(Pro-Hyp-Gly) which is sterilized by an electron beam and observed its effect on expression of target genes *in vitro* and *in vivo*. We found that the siRNA/SYCOL complex solution has a gene silencing activity in culture cells, mouse muscles, and xenografted tumors. Thus, we concluded that even a simple synthetic collagen can deliver siRNA into cells *in vivo* and *in vitro*.

Materials and methods

Collagens

In vivo siRNA transfection kit of AteloGene for systemic use containing Atelocollagen (ATCOL) (concentration 0.1%) or for local use (ATCOL concentration 1%) was purchased from KOKEN and used according to the manufacturer's instructions. We obtained a synthetic collagen poly(Pro-Hyp-Gly) (SYCOL), molecular weights greater than 10^5) made by polycondensation of Pro-Hyp-Gly as a gift by Chisso, which was sterilized by irradiation of an electron beam (40KG) for 2 min (Sanshodoh).

Preparation of siRNA

Synthetic 21-nt RNAs were purchased from KOKEN. The sequences of the mouse growth differentiation factor (DGF)-8 (myostatin) siRNA are 5′-AAGAUGACGAUUAUCACGCUA-3′ and 3′-UUCUACUGCUAAUAGUGCGAU-5′.

The control sequences of scramble siRNA are 5′-AUCGAAUAACCGUAACGUUGA-3′ and 3′-UAGCUUAUUGGCAUUGCAACU-5′. The control siRNA duplex and Firefly luciferase GL3 siRNA duplex were purchased from Nippon gene.

Formation of siRNA/synthetic collagen complex

The siRNAs and the collagen complexes were prepared as follows. Equal volumes of collagen (in phosphate buffered saline (PBS) at pH 7.4) and siRNAs solution were combined and mixed by vigorous pipetting. The final concentration of the collagen was 0.03%. The complex was then kept at 4°C for 16 h before use.

Stability tests of siRNA/collagen complex

An aliquot of 0.9 μg of siRNAs (luciferase GL3 duplex) complexed with lipofectamin 2000 (Invitrogen), ATCOL (concentration 0.5%), ATCOL (0.05%) or SYCOL (0.03%) was incubated in the presence of 0.1 μg/μL RNase A (Nippon gene) for 0, 5, 15, 30, 45 and 60 min at 37°C. The siRNAs were extracted from the reaction solution with phenol and phenol/chloroform/isoamyl alcohol (25:24:1). Then, the siRNAs were precipitated with ethanol and polyacrylamide gel electrophoresed (25%) and visualized by ethidium bromide staining.

Cell lines

B16-F10-luc-G5 melanoma cells continuously expressing luciferase (Xenogen) were maintained in Dulbecco's Modified Eagle Medium (DMEM) with 10% heat-inactivated fetal bovine serum (FBS) and Zeocin (0.2 mg/mL) at 37°C in a humidified atmosphere of 5% CO_2.

Synthetic collagen-mediated siRNA transfer

The siRNA/SYCOL (0.03%) complexes were prefixed to a 24 well plate (10–173 pmol siRNA/50 μL/well) according to the method described previously (Minakuchi *et al.* 2004). The cultured cells were plated into the complex-prefixed 24 well plate at 3.5×10^4 B16-F10-luc-G5 melanoma cells/well and the effects of siRNA transfer were then measured by a luciferase assay. The cationic liposome-mediated transfer of siRNA was performed as described by the manufacturer (Invitrogen).

Luciferase assays

For luciferase-based reporter gene assays, B16-F10-luc-G5 cells were used. The cells were collected by trypsinization and plated in the 24-well dishes for siRNA transfection. SYCOL- or ATCOL-mediated or conventional transfection of siRNAs into cells was performed in accordance with the manufacturer's instructions. Cells were lysed (n = 3) on day 2 and analyzed for luciferase activity (Microplate reader Model 680; Bio-Rad).

Effects of SYCOL-mediated local transfer of siRNA against myostatin in muscles

siRNAs against *Myostatin* (final concentration, 10 μM) were mixed with SYCOL (final concentration for local administration, 0.03%) or ATCOL (0.05%) according to the manufacturer's instructions. After anesthesia of mice (20-week-old male C57BL/6) by Nembutal (25 mg/kg, i.p.), the myostatin siRNA/SYCOL (myostatin-siRNA/SYCOL) complex was injected into the masseter on the left side. As a control, scrambled siRNA/SYCOL complex was injected into the contralateral (right) muscles. After 2 weeks, the muscles on both sides were isolated and processed for analysis.

Real-time quantitative RT–PCR

Total RNA was extracted from the masseter muscle, and reverse transcribed. Transcript levels of *myostatin* were measured using DNA Engine OPTICON system (Bio-Rad) with SYBR Premix Ex Tag (Takara Shuzo). The specific primers used were as follows; 5′-CAG CCT GAA TCC AAC TTA GG-3′ (Forward primer, region 758), 3′-TCG CAG TCA AGC CCA AAG TC-5′ (Reverse Primer, region 905).

Monitoring luciferase inhibition in vivo *with bioluminescent imaging*

B16-F10-luc-G5 cells were subcutaneously injected (1×10^6 cells/100 μL) into athymic nude mice inferior ophthalmic vein of right eye. Seven days later, 200 μL of each solution containing luciferase GL3 siRNA/ATCOL (0.05%), luciferase GL3 siRNA/SYCOL (0.03%), SYCOL alone, or luciferase GL3 siRNA alone was injected into the mouse inferior ophthalmic vein of the left eye. For *in vivo* imaging, D-luciferin (150 mg/kg; WAKO) was injected into the mouse inferior ophthalmic vein of the right eye. Fifteen minutes later, photons from animal whole bodies were counted by using the IVIS imaging system (Xenogen) according to the manufacturer's instructions. Data were analyzed by using LIVINGIMAGE 2.50 software (Xenogen). A successful injection was indicated by day 0 images that showed a systemic bioluminescence distributed throughout the animal, and only those mice evidencing a satisfactory injection were used in the continued experiment. The siRNA/SYCOL and siRNA/ATCOL effects were monitored after 3 days *in vivo* by bioluminescent imaging. Tumor growth was not affected by these treatments.

For preparing the siRNA/SYCOL complex, an equal volume of SYCOL (0.06% in distilled water at pH 5.6) and siRNA solution was combined and mixed by rotating for 20 min at 4°C. For preparing the siRNA/ATCOL complex, equal volumes of ATCOL (0.1% in siRNA buffer by KOKEN) and siRNA solution were combined and mixed by rotating for 20 min at 4°C. The siRNAs or their complexes were directly injected into the mouse inferior ophthalmic vein of the left eye. The final concentrations of SYCOL and ATCOL were 0.03% and 0.05%, respectively. The siRNA concentration used in the liposome experiments was 4 nmol/mouse equivalent to that used in the SYCOL or ATCOL experiments. *In vivo* bioimaging was conducted on a cryogenically cooled IVIS system (Xenogen) using LivingImage acquisition and analysis software (Vooijs *et al.* 2002).

Statistical analysis

The results are given as means ± standard error (SE). Statistical analysis was conducted using the analysis of variance with the Bonferroni correction for multiple comparisons. A *P*-value of 0.05 or less was considered to indicate a significant difference.

Results

In vitro *delivery of siRNA with a synthetic collagen poly(Pro-Hyp-Gly)*

In the case of Atelocollagen (ATCOL), it has been reported that the siRNA (luciferase GL3 duplex)/ATCOL complex shows resistance to degradation of siRNA in the presence of RNase A (Minakuchi *et al.* 2004). To examine whether a synthetic collagen poly(Pro-Hyp-Gly) (SYCOL) can block degradation of siRNA (luciferase GL3 duplex) from the RNase, siRNA/SYCOL complex solution was incubated in the presence of the RNase (0.1 μg/μL) for 0, 5, 15, 30, 45 and 60 min at 37°C. For comparison, the same experiment was carried out with naked siRNA, siRNA/liposome complex and siRNA/ATCOL complex. Results obtained by polyacrylamide gel electrophoresis (PAGE) are shown in Fig. 1, where the siRNA/SYCOL (0.03%) complex showed partial resistance to degradation of siRNA by the RNase, similarly to the siRNA/ATCOL (0.05%) complex, although the SYCOL complex (0.03%) was less resistant than the siRNA/ATCOL (a high concentration 0.5%) and the liposome complex. We attempted to perform the same experiments in higher concentrations of SYCOL. However, since heavy precipitation in a stock solution of SYCOL was observed in a higher concentration than 0.06%, we could not estimate the resistance in higher concentration than 0.03%.

Next, we compared the efficiency of the SYCOL-mediated transfer activity with that of the ATCOL-mediated one. To examine whether SYCOL has an activity

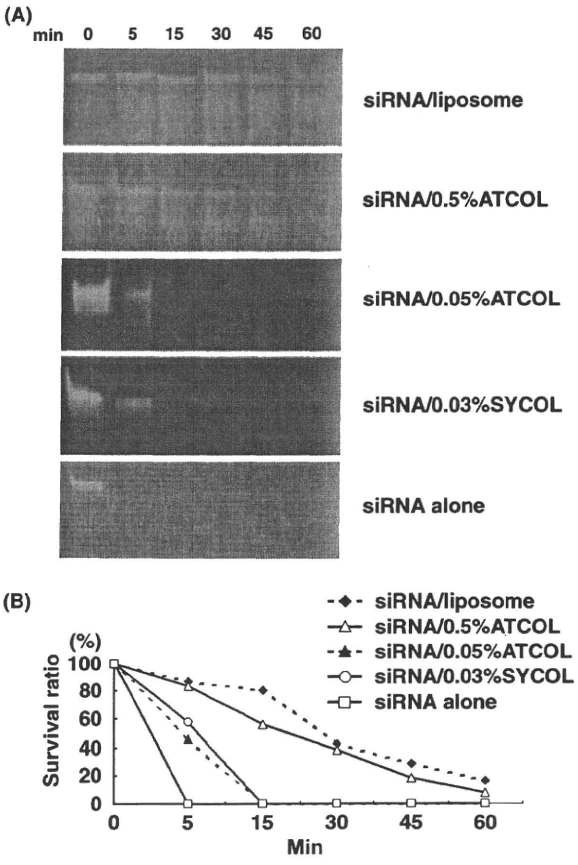

Fig. 1. A synthetic collagen poly(Pro-Hyp-Gly) (SYCOL) protects degradation of small interfering RNA (siRNA) (luciferase GL3 duplex) by RNase A. (A) siRNA (luciferase GL3 duplex)/liposome, siRNA/Atelocollagen (ATCOL) (0.5%), siRNA/ATCOL (0.05%), siRNA/SYCOL (0.03%) complexes or naked siRNA were incubated in the presence of RNase A for 0, 5, 15, 30, 45 and 60 min at 37°C and then polyacrylamide gel electrophoresed. Ethidium bromide staining revealed the presence of siRNA. (B) siRNA survival ratio (0 min, 5 min, 15 min, 30 min, 45 min or 60 min/0 min of fluorescence ratio) of RNA fragment fluorescence emitted from electrophoretic gels. Software of ImageJ (NIH, USA) was used for measurement of fluorescence intensity.

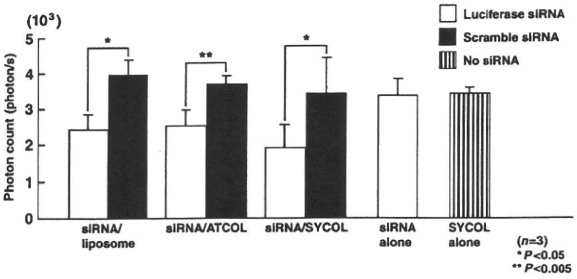

Fig. 2. A synthetic collagen poly(Pro-Hyp-Gly) (SYCOL) can transfer siRNA into cells. The luciferase siRNA duplexes were transfected into the B16-F10-luc-G5 melanoma cells to measure inhibitory effects on luciferase production of B16-F10-luc-G5 melanoma cells. Luciferase activity was measured at day 2 after transfection of siRNA/liposome, siRNA/ATCOL, siRNA/SYCOL complexes, naked siRNA or SYCOL (0.03%) solutions. White bar, luciferase siRNA; Black bar, scramble siRNA; Striped pattern bar, no siRNA.

of siRNA delivery into cells, we used a luciferase reporter gene system in B16-F10-luc-G5 melanoma cells, which continuously expresses luciferase (*luc*) as a well-characterized target of siRNA. In this culture system, the siRNA (luciferase GL3 duplex)/SYCOL complex was pre-coated on a micro-well plate on which the cells were then seeded (Minakuchi *et al.* 2004). Using a *luc* assay, photon emission was detected as photon counts by a luminometer. The photon counts decrease when the cells were treated with the siRNA against *luc* complexed with the SYCOL as well as with ATCOL or with a liposome (Fig. 2), while no significant difference was observed in the presence of either siRNA (luciferase GL3 duplex) against *luc* alone or SYCOL alone (Fig. 2). These data indicated that the siRNA/SYCOL complex was incorporated into the cells and the siRNA can knockdown the *luc* expression as efficiently as in the presence of ATCOL or the conventional liposome. Taken together, these data showed that SYCOL can protect siRNA against RNase A and that the siRNA/SYCOL complex was able to exhibit a gene silencing effect *in vitro* as efficiently as the siRNA/ATCOL complex.

Effects of SYCOL-mediated local transfer of siRNA against myostatin in muscles

As one of the practical platforms for siRNA delivery, we previously adopted an ATCOL-mediated siRNA delivery system to apply myostatin-targeting siRNA into muscles and demonstrated that local or systemic applications of siRNA against myostatin complexed with ATCOL markedly stimulated muscle growth *in vivo* within a few weeks (Kinouchi *et al.* 2008). In order to compare efficiency of the local transfer of siRNA into muscles between SYCOL and ATCOL complexes, we performed the same experiments with SYCOL instead of using ATCOL, as reported previously (Kinouchi *et al.* 2008). We prepared the nano-particle complex containing the siRNA against *myostatin* (10 μM) and SYCOL. Then, we injected the myostatin-siRNA/SYCOL complex into the masseter muscle of 20-week-old C57BL/6 mice. As a control, we injected scrambled siRNAs/SYCOL complex in the contralateral muscle. Two weeks after injection, we

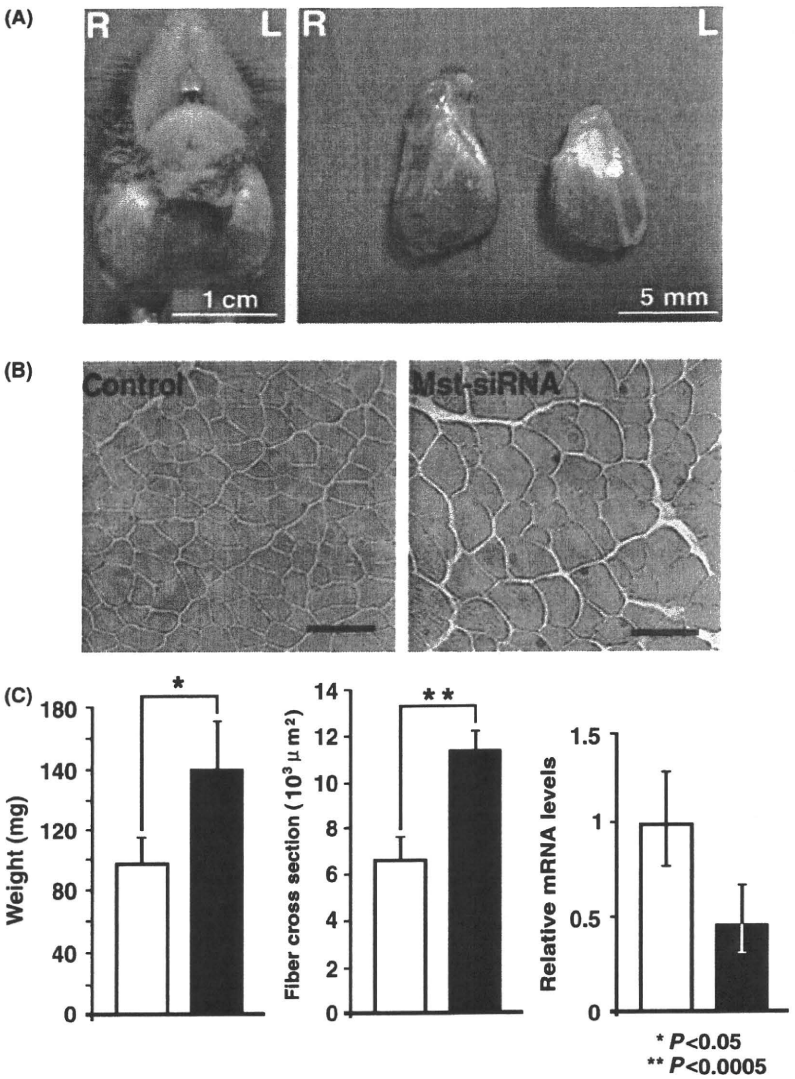

Fig. 3. Local treatment of myostatin-siRNA/synthetic collagen poly(Pro-Hyp-Gly) (SYCOL) makes the masseter muscle large in mice. Myostatin-siRNA/SYCOL treatment improves myofibril size in C57BL/6 mice. (A) Photographs of the muscles. The masseter muscles injected intramuscularly with the myostatin-siRNA/SYCOL complex show a marked increased muscle mass in 20-week-old C57BL/6 mice. (B) Hematoxylin and eosin staining of the control and myostatin-siRNA/SYCOL-treated masseter muscles. Muscles were cut to make frozen sections (5 μm thickness) at the mid-belly of the muscle and stained. Scale bar, 50 μm. (C) Average values of weights (left) and myofibril sizes (center), and the ratio of the amount of myostatin mRNA (right) for the masseter muscles. White bar, control muscles; Black bar, myostatin-siRNA/SYCOL-treated muscles.

observed gross morphology of the muscles and dissected the muscle tissues. After injection of the myostatin-siRNA/SYCOL complex, the masseter muscle (on the left side) was enlarged, while no significant change was observed on the contralateral side (Fig. 3A). Histological analysis showed that the myofibril sizes of the masseter muscles treated with the myostatin-siRNA/SYCOL complex were larger than those of the control (Fig. 3B). We also measured the muscle weight, finding that the myostatin-siRNA/SYCOL-treated muscles weighed significantly more than those on the control side (Fig. 3C, left). Examining the sizes of 200 myofibers per each group, the population of myofibril sizes indicated a shift from smaller to larger fibers in the myostatin-siRNA/SYCOL-treated muscles. The average myofibril size of the muscle treated with myostatin-siRNA/SYCOL gained approximately 1.8 times more than that of control (Fig. 3C, center), showing muscle hypertrophy. To confirm that siRNA decreased the amount of myostatin mRNA in the masseter muscle, we performed quantitative PCR (q-PCR) (Fig. 3C, right). We estimated the ratio of the amount of myostatin mRNA in the siRNA-treated muscle compared with the contralateral muscle (n = 4). The average ratio in the treated muscle was lowered to 0.48 ± 0.11 (in triplicate, ± standard error), indicating that RNAi had occurred. No obvious morphological change was observed in other tissues than the treated masseter muscle. In the meantime, we did not observe any general sign of ill health and deaths during the experimental period, indicating that the siRNA complex gives no obvious adverse effects. The increase of the myostatin-siRNA/SYCOL-treated muscle mass indicated that the SYCOL system can be

used to induce a target-gene specific RNAi *in vivo* as well as the ATCOL system (Kinouchi *et al.* 2008).

Effects of intravenous administration of the siRNA/SYCOL complex in mice

To examine whether SYCOL-mediated siRNA transfer is valid for systemic gene silencing, we used mice bearing a Luc-producing melanoma described previously (Minakuchi *et al.* 2004). We carried out non-invasive *in vivo* bioluminescence imaging analysis to measure luminescence intensity (photon/s) in the tumor of mice injected with the siRNA alone, the siRNA/SYCOL complex, or siRNA/ATCOL complex (Fig. 4A). The luminescence in the tumor was observed in the head (injected site) and the abdomen at 0 day. After injection of siRNA alone or SYCOL alone, the luminescence became intense in both head and abdomen at 3 days after injection. In contrast, mice administered with the siRNA/ATCOL complex showed a relatively low intensity of the luminescence at 3 days after injection as observed by Minakuchi *et al.* (2004). In the case of the siRNA/SYCOL complex, the luminescence intensity increases in the abdomen (Fig. 4A,B), but decreases in the head region, showing sustained inhibition of luciferase expression in the head region (Fig. 4A,C). These results suggested that this SYCOL-mediated *in vivo* transfer of siRNA could be valid locally in tissues around an injected region.

Discussion

Knockdown of gene expression by RNAi becomes a powerful tool for the genetic analysis both *in vitro* and *in vivo*, while how to deliver siRNAs to the target cells and tissues has been a major challenge for RNAi based researches (Tiemann & Rossi 2009). In order to develop effective non-vector-based siRNA delivery systems for the future of siRNA-based research and therapies, we have used an ATCOL-mediated siRNA transfer systems *in vitro* and *in vivo*, because ATCOL allowed increased cellular uptake, nuclease resistance and prolonged release of siRNAs (Minakuchi *et al.* 2004). However, so far we have not known mechanisms underlying the ATCOL-mediated transfer of siRNA. In order to elucidate the mechanisms, we selected a simple synthetic collagen and examined whether it has transfer ability of siRNA into cells. Tanihara and his group developed synthetic collagen fibers poly(Pro-Hyp-Gly) (SYCOL) consisting of the Pro-Hyp-Gly sequence by direct polycondensation of Pro-Hyp-Gly tripeptides (Kishimoto *et al.* 2005). SYCOL is a polypeptide, has molecular weights greater than 10^5 and forms triple-helical, but is thermally stable up to

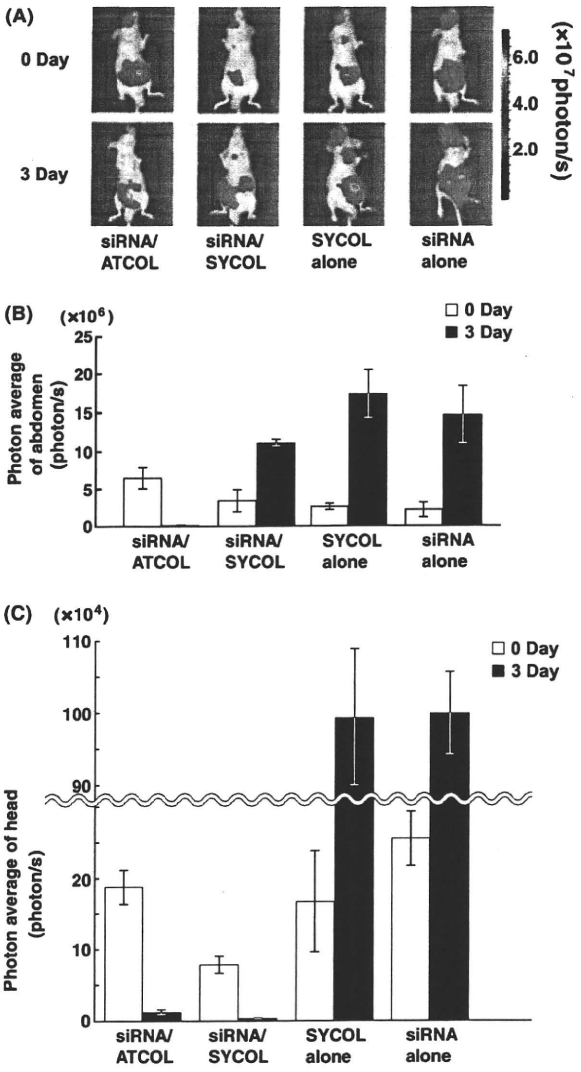

Fig. 4. Monitoring luciferase inhibition *in vivo* with bioluminescent imaging. (A) Representative images of nude mice at 3 days after tumor injection into the left ventricle of the eye with 1×10^6 B16-F10-luc-G5 cells suspended in 100 μL of sterile phosphate-buffered saline (PBS). Each animal was given i.v. with 200 μL of 25 μg of GL3 siRNA/ATCOL complex, GL3 siRNA/SYCOL complex, SYCOL (0.03%) solution or luciferase GL3 siRNA. (B) Photon averages of bioluminescence emitted from the abdominal region. (C) Photon averages from the head region. White bar, photon averages at 0 day; Black bar, photon averages 3 days.

80°C and it contains no pathogens. In the present study, when we used SYCOL, a poly(Pro-Hyp-Gly) sterilized with electron-beam irradiation, instead of ATCOL, we observed significant gene-silencing effects with siRNA. Although at first we considered that only natural collagens have the ability of gene transfer, we demonstrated here that SYCOL has an activity of

silencing gene expression with siRNA. We speculate a structure of the siRNA/SYCOL complex in a buffer as follows. When SYCOLs are mixed with siRNA molecules, their terminal cationic groups may spontaneously make complex with siRNA by electrostatic interaction and form a protective outer layer that shields siRNA core, giving rise to the steric stabilization of the polyplex structure against undesirable interactions with impertinent surroundings. Since a desirable polymer structure for *in vivo* delivery purposes is a sterically stabilized but neutral, not positively charged nanoparticle (Gary *et al.* 2007), the siRNA/SYCOL complex may be a desirable one.

We also speculate a mechanism underlying cellular uptake of the siRNA/SYCOL complex as follows. Since it is known that degradation of collagen occurs primarily through a phagocytic pathway, which is required for the physiological remodeling of connective tissues during growth and development (Lee *et al.* 2007), cells may incorporate the siRNA/SYCOL complex into the cytosol probably by endocytosis.

In the case of intravenous administration of the siRNA/SYCOL complex in mice, unexpectedly we observed the silencing effect only in the head region, but not in the abdominal region. This may indicate that SYCOL itself may be somehow changed or decomposed more rapidly in blood than ATCOL and then siRNA may be released in blood. If this is the case, due to low stability of SYCOL in the blood, this RNAi is not systemic and may be induced around injected local area (in the head region, but not in the abdominal region in the present experiment).

One technical problem associated with siRNA transfer *in vivo* is the targeting of siRNA delivery to a specific tissue. For this purpose, the present SYCOL-based transfer method has great potential for site-specific transportation of target siRNAs either by way of local injection or intravenous administration. Furthermore, since SYCOL is easily modified so as to be incorporated in specific cells or tissues, for instance, to facilitate uptake by targeting cells, SYCOL could be modified chemically by conjugating with cell-targeting antibodies or ligands (Kim & Kim 2009), we may find some structures of SYCOL that are more suitable for increasing efficiency of siRNA-delivery *in vivo*.

In conclusion, we demonstrated that the siRNA/SYCOL complex is very useful to obtain gene-silencing effects. Since we can design structures of synthetic collagens, we may screen various synthetic collagens to achieve maximal function of siRNA-based gene silencing *in vivo*. Thus, a SYCOL-based siRNA transfer system represents an attractive method for local administration of siRNA and has potential for delivery of siRNA into specific cells or tissues and thus probably for clinical applications of RNAi.

Acknowledgments

The authors thank Kawasaki Medical School for technical and financial supports. This work was supported partially by a Research Grant 20B-13 for Nervous and Mental Disorders and a Research Grant for Research on Psychiatric and Neurological Diseases and Mental Health from the Ministry of Health, Labour and Welfare.

References

Behlke, M. A. 2006. Progress towards *in vivo* use of siRNAs. *Mol Ther*. **13**, 644–670.

Gary, D. J., Puri, N. & Won, Y. Y. 2007. Polymer-based siRNA delivery: perspectives on the fundamental and phenomenological distinctions from polymer-based DNA delivery. *J. Control Release* **121**, 64–73.

Kim, S-S., Garg, H., Joshi, A. & Manjunath, N. 2009. Strategies for targeted nonviral delivery of siRNAs *in vivo*. *Trends Mol. Med*. **15**, 491–500.

Kim, W. & Kim, S. 2009. Efficient siRNA Delivery with Non-viral Polymeric Vehicles. *Pharm. Res.* **26**, 657–666.

Kinouchi, N., Ohsawa, Y., Ishimaru, N., Ohuchi, H., Sunada, Y., Hayashi, Y., Tanimoto, Y., Moriyama, K. & Noji, S. 2008. Atelocollagen-mediated local and systemic applications of myostatin-targeting siRNA increase skeletal muscle mass. *Gene Ther*. **15**, 1126–1130.

Kishimoto, T., Morihara, Y., Osanai, M., Ogata, S., Kamitakahara, M., Ohtsuki, C. & Tanihara, M. 2005. Synthesis of poly(Pro-Hyp-Gly)(n) by direct poly-condensation of (Pro-Hyp-Gly)(n), where n = 1, 5, and 10, and stability of the triple-helical structure. *Biopolymers* **79**, 163–172.

Lee, H., Sodek, K. L., Hwang, Q., Brown, T. J., Ringuette, M. & Sodek, J. 2007. Phagocytosis of collagen by fibroblasts and invasive cancer cells is mediated by MT1-MMP. *Biochem. Soc. Trans.* **35**, 704–706.

Minakuchi, Y., Takeshita, F., Kosaka, N., Sasaki, H., Yamamoto, Y., Kouno, M., Honma, K., Nagahara, S., Hanai, K., Sano, A., Kato, T., Terada, M. & Ochiya, T. 2004. Atelocollagen-mediated synthetic small interfering RNA delivery for effective gene silencing *in vitro* and *in vivo*. *Nucleic Acids Res.* **32**, e109.

Ochiya, T., Nagahara, S., Sano, A., Itoh, H. & Terada, M. 2001. Biomaterials for gene delivery: atelocollagen-mediated controlled release of molecular medicines. *Curr. Gene Ther.* **1**, 31–52.

Stenzel, K. H., Miyata, T. & Rubin, A. L. 1974. Collagen as a Biomaterial. *Annu. Rev. Biophys. Bioeng.* **3**, 231–253.

Tiemann, K. & Rossi, J. J. 2009. RNAi-based therapeutics-current status, challenges and prospects. *EMBO Mol. Med*. **1**, 142–151.

Vooijs, M., Jonkers, J., Lyons, S. & Berns, A. 2002. Noninvasive imaging of spontaneous retinoblastoma pathway-dependent tumors in mice. *Cancer Res.* **62**, 1862–1867.